

1 **GROWTH-RATE DEPENDENT AND NUTRIENT-SPECIFIC GENE
2 EXPRESSION RESOURCE ALLOCATION IN FISSION YEAST**

3 Istvan T. Kleijn^{1,2,3,*}, Amalia Martínez-Segura^{1,2,*}, François Bertaux^{1,2,3,§}, Malika Saint^{1,2},
4 Holger Kramer^{1,2}, Vahid Shahrezaei^{3,4}, & Samuel Marguerat^{1,2,4}

5

6 ¹ MRC London Institute of Medical Sciences (LMS), Du Cane Road, London W12 0NN, UK

7 ² Institute of Clinical Sciences (ICS), Faculty of Medicine, Imperial College London, Du Cane Road,
8 London W12 0NN, UK

9 ³ Department of Mathematics, Faculty of Natural Sciences, Imperial College London, London SW7 2AZ,
10 UK

11 ⁴ Correspondence to v.shahrezaei@imperial.ac.uk or samuel.marguerat@imperial.ac.uk

12 * These authors contributed equally to this work.

13 [§] Present address: Institut Pasteur, 28 rue du Docteur Roux, 75015 Paris, France.

14

1 **ABSTRACT**

2 Cellular resources are limited and their relative allocation to gene expression programmes
3 determines physiological states and global properties such as the growth rate. Quantitative
4 studies using various growth conditions have singled out growth rate as a major physiological
5 variable explaining relative protein abundances. Here, we used the simple eukaryote
6 *Schizosaccharomyces pombe* to determine the importance of growth rate in explaining relative
7 changes in protein and mRNA levels during growth on a series of non-limiting nitrogen
8 sources. Although half of fission yeast genes were significantly correlated with the growth rate,
9 this came alongside wide-spread nutrient-specific regulation. Proteome and transcriptome
10 often showed coordinated regulation but with notable exceptions, such as metabolic enzymes.
11 Genes positively correlated with growth rate participated in every level of protein production
12 with the notable exception of RNA polymerase II, whereas those negatively correlated mainly
13 belonged to the environmental stress response programme. Critically, metabolic enzymes,
14 which represent ~55-70% of the proteome by mass, showed mainly condition-specific
15 regulation. Specifically, many enzymes involved in glycolysis and NAD-dependent metabolism
16 as well as the fermentative and respiratory pathways were condition-dependent and not
17 consistently correlated with growth. In summary, we provide a rich account of resource
18 allocation to gene expression in a simple eukaryote, advancing our basic understanding of the
19 interplay between growth-rate dependent and nutrient-specific gene expression.

20

21

1 **INTRODUCTION**

2 Cellular growth is the process by which cells increase in mass. It is a fundamental systemic
3 process that impacts most aspects of cell physiology. Growth can be very fast: for example,
4 yeast cells can double in mass every few hours, and certain bacteria only require minutes.
5 Conversely, slower growth is observed in multicellular organisms, in which several cell types
6 take days to grow and divide. Crucially, the cellular growth rate changes in response to
7 external cues such as nutrient quality, stressing agents, or growth factors.

8 Measurements of biomass composition in unicellular organisms have long-established cellular
9 growth rates as a covariate of cell physiology (Schaechter, Maaløe, and Kjeldgaard 1958;
10 Mitchison and Lark 1962; Waldron and Lacroute 1975; Fantes and Nurse 1977; Neidhardt,
11 Ingraham, and Schaechter 1990; Bremer and Dennis 2008). In the last decade, quantitative
12 experimental work, together with mathematical modelling, have described this relationship
13 (reviewed in (Klumpp and Hwa 2014; Shahrezaei and Marguerat 2015; Jun et al. 2018;
14 Bruggeman et al. 2020)). This body of work has emphasised how the macromolecular
15 composition of the cell is tightly connected to growth rate. Specifically, for cultures undergoing
16 balanced exponential growth modulated by external nutrients, the total RNA abundance per
17 unit of biomass and the growth rate are correlated linearly. This phenomenological relationship
18 is called the first or ribosomal growth law and reflects an increased requirement for ribosomes
19 during faster growth to support protein synthesis. The demand for ribosomes is also felt at the
20 protein level, where it induces a trade-off between proteins involved in translation and those
21 involved in catabolism. It was shown that about half of the total protein mass in *Escherichia*
22 *coli* responded to growth modulations by nutrient limitation and translational inhibition (Scott
23 et al. 2010; You et al. 2013). These observations were formalised in a phenomenological
24 model separating the proteome into three broad sectors based on their growth rate
25 correlations. Proteins that are positively correlated with the cellular growth rate during nutrient
26 limitation and negatively during translational inhibition comprise the R-sector, whereas
27 proteins showing the opposite behaviour comprise the P-sector. Proteins that do not respond
28 to the growth rate belong to the Q-sector (Scott et al. 2010). The concept of proteome sectors
29 has been the basis of several phenomenological and coarse-grained mechanistic models
30 relating optimal resource allocation to protein abundance and cellular growth rates (Molenaar
31 et al. 2009; Scott et al. 2014; Maitra and Dill 2015; Weiße et al. 2015; Pandey and Jain 2016;
32 Liao, Blanchard, and Lu 2017; Bertaux et al. 2020; Hu et al. 2020).

33 The molecular mechanisms behind the phenomenological assignment to the three proteome
34 sectors remain less well understood. R-sector proteins are universally involved in translation
35 and ribosome biogenesis and many of them are controlled by global signalling pathways such
36 as guanosine tetraphosphate (ppGpp) in prokaryotes or the target of rapamycin complex 1

1 (TORC1) in eukaryotes (Irving, Choudhury, and Corrigan 2020; Petibon et al. 2020). P-sector
2 proteins, on the other hand, are more diverse and often involved in metabolic adaptation and
3 stress response (Brauer et al. 2008; You et al. 2013; Hui et al. 2015; A. Schmidt et al. 2016).
4 In *E. coli*, the master regulator CRP-cAMP has been proposed to control the P-sector
5 assignments of carbon catabolism enzymes when growth rate was modulated by the quality
6 of abundant carbon sources (You et al. 2013). Under other growth modulations and in other
7 organisms, whether the regulation of P-sector proteins is as directly mechanistically linked to
8 the growth rate as for R-proteins is less clear.

9 Transcriptomics and proteomics have been instrumental in characterising the coordination
10 between gene expression and cellular growth. The ribosomal growth law was first confirmed
11 in the *E. coli* proteome in continuous cultures limited by carbon availability (Peebo et al. 2015),
12 under titrations of carbon, nitrogen, and translational inhibition (Hui et al. 2015), and in an
13 extensive study of 22 growth conditions (A. Schmidt et al. 2016). In addition, the Hui study
14 proposed that the P sector could be divided into subsectors related to different metabolic
15 functions depending on the type of nutrient limitation. In the budding yeast *Saccharomyces*
16 *cerevisiae*, a seminal microarray study showed strong correlations between hundreds of
17 transcripts with the chemostat dilution rate across six nutrient titrations (Brauer et al. 2008).
18 The observed correlations agreed with the ribosomal growth law and highlighted stress
19 response as a component of the P-sector alongside metabolic functions. More recently, Metzl-
20 Raz and colleagues observed the ribosomal growth law in the proteome of budding yeast after
21 combining existing data sets of cultures grown in a variety of carbon sources (Paulo et al.
22 2015; 2016) with data obtained under nitrogen and phosphorus limitation (Metzl-Raz et al.
23 2017). They also proposed that a pool of non-translating ribosomes is available as a buffer
24 during changing growth conditions, a strategy also observed in prokaryotes (Dai et al. 2016;
25 Mori et al. 2017; Kohanim et al. 2018). This suggest that resource allocation may not be fully
26 optimised for maximal cell growth. Signs of excess capacity have also been reported for
27 metabolic pathways, including glucose catabolism (Yu et al. 2020). Further omics studies in
28 *S. cerevisiae* have defined additional characteristics of resource allocation such as
29 reallocation of proteome mass from amino acid biosynthesis to protein translation upon amino
30 acid supplementation (Björkeroth et al. 2020), or the respective contribution of transcription
31 and translation to different allocation strategies (Yu et al. 2021). Thus, genome-wide omics
32 experiments have been key to improve our understanding of resource allocation in *E. coli* and
33 *S. cerevisiae* by connecting proteome sectors to specific physiological functions.

34 The cellular growth rate reflects the metabolic state of the cell and in limiting nutrient conditions
35 metabolic enzymes are often part of the P-sector (Hui et al. 2015; A. Schmidt et al. 2016). This
36 suggests that expression levels of specific metabolic enzymes when responding to external

1 conditions can be directly regulated alongside the growth rate. The cell metabolism however
2 is an exquisitely complex network of interconnected processes and perturbation of single
3 pathways can have wide-spread systemic effects. Central carbon metabolism (CCM) relies on
4 three pathways: glycolysis, the pentose phosphate pathway, and the tricarboxylic acid (TCA)
5 cycle. Together, these generate energy in the form of ATP, in a process mediated by reducing
6 agents such as NADH, and produce building blocks for biosynthesis. ATP can be generated
7 anaerobically via fermentation; a process which consists of glycolysis and the subsequent
8 degradation of pyruvate, or aerobically via respiration, which requires the TCA cycle and
9 subsequent oxidative phosphorylation (OXPHOS). The extent of fermentative versus
10 respiratory metabolism affects the NAD+/NADH redox balance and vice versa, as NAD+
11 reduction during glycolysis and the TCA cycle must be balanced by NADH oxidation occurring
12 during pyruvate degradation and OXPHOS (Vemuri et al. 2007; van Hoek and Merks 2012;
13 Campbell et al. 2018; Luengo et al. 2020). In eukaryotes, these reactions are
14 compartmentalised between the cytoplasm and the mitochondria, with the latter housing the
15 respiratory enzymes and functioning as hubs that connect diverse metabolic pathways
16 including CCM and amino acid metabolism (Spinelli and Haigis 2018). For instance, amino
17 acid degradation enables the assimilation of nitrogen as ammonium or glutamate via de- or
18 transamination reactions. The remaining carbon backbone is recycled into the cell's biomass
19 or excreted, and the associated metabolites affect carbon metabolism (Godard et al. 2007).
20 Importantly, mitochondrial intermediates are required for amino acid biosynthesis even during
21 fermentative energy generation (Malecki et al. 2020). In fission yeast, a single point mutation
22 in the pyruvate kinase Pyk1, affecting its activity, has been shown to rebalance the fluxes
23 through the fermentation and respiration pathways alongside shifts in the transcriptome and
24 proteome composition (Kamrad et al. 2020), giving a prime example of how the cell co-adjusts
25 perturbations in metabolic fluxes and expression burdens. Taken together, shifts in the
26 metabolic demand propagate throughout the cell, as most metabolic pathways are tightly
27 interlinked (Chubukov et al. 2014).

28 The expression levels of CCM enzymes, and therefore the fluxes through the pathways
29 depend on external conditions and stress levels. As a result, cellular states and metabolic
30 strategies are linked to resource allocation to different gene expression programmes. For
31 example, during rapid growth on glucose, yeast utilises the fermentative pathway alongside
32 the TCA cycle even in the presence of oxygen, a phenomenon known as aerobic glycolysis or
33 the Crabtree effect (Shimizu and Matsuoka 2018). Aerobic glycolysis is also a characteristic
34 of tumour cells, for which it is known as the Warburg effect (Heiden, Cantley, and Thompson
35 2009). This strategy appears counterintuitive as fermentation generates fewer molecules of
36 ATP per glucose molecule than respiration. Several hypotheses have been proposed to

1 resolve this paradox. All require a second growth-limiting constraint besides glucose uptake
2 which would be specific to respiro-fermentative growth (de Groot et al. 2019). Examples
3 include the cytoplasmic density of macromolecules (Vazquez et al. 2008; Goelzer et al. 2015),
4 total proteome allocation (Basan et al. 2015), and membrane area availability (Szenk, Dill, and
5 de Graff 2017). Thus, a whole-cell understanding of cellular trade-offs between multiple
6 constraints must take into account gene expression alongside metabolic maps (Goelzer and
7 Fromion 2017; Yang et al. 2018; Dahal, Zhao, and Yang 2020). Resource allocation
8 constraints have been successfully introduced into genome-wide metabolic models of several
9 organisms as more high-quality expression data has become available (O'Brien et al. 2013;
10 Sánchez et al. 2017; Y. Chen et al. 2020). In summary, quantitative surveys of the gene
11 expression cost of metabolic pathways are key to understanding cell physiology.

12 Here, we define the growth-rate dependent and nutrient-specific resource allocation to the
13 fission yeast *Schizosaccharomyces pombe* proteome and transcriptome. We find that both
14 types of regulation are interconnected and define protein synthesis and stress response as
15 the processes positively and negatively regulated with the growth rate. We then study the
16 plasticity of the gene expression burden of metabolic pathways in response to changes in
17 nutrients and their reliance on transcriptional and post-transcriptional regulation. Altogether
18 we provide a rich account of resource allocation in a simple eukaryote as a function of external
19 conditions.

20 RESULTS

21 **Fission yeast gene expression shows growth-rate-related and condition-specific 22 components**

23 To generate cell populations that grow at different rates while not limited for nutrients, we used
24 eight defined culture media each containing a unique source of nitrogen. These media have
25 been extensively characterised elsewhere (Fantes and Nurse 1977; Carlson et al. 1999;
26 Petersen and Russell 2016). Seven media contained 20 mM of a single amino acid (Trp, Gly,
27 Phe, Ser, Ile, Pro, Glu), and one 93.5 mM of ammonium chloride (NH₄Cl, referred to as Amm)
28 as a reference (**Fig. 1**). In our hands, this design achieved growth rates ranging 0.05 - 0.28 h⁻¹. *S. pombe* 972h⁻ prototroph wild-type cells were grown in turbidostats at constant
30 concentrations of OD₆₀₀ ~0.4 (3 - 5×10⁶ cells/ml) in triplicates for 43 - 143 h (6 - 28 generations
31 depending on the nitrogen source) (**Fig. 1C-E, Supp. Table S1**) (Takahashi et al. 2015). Like
32 in chemostats, turbidostat cultures are diluted by the addition of fresh media. In the case of
33 the turbidostat system, however, it is the cell concentration that is directly measured and
34 maintained constant and not the proliferation rate. This ensures that cellular growth is not
35 limited by a lack of nutrients, but rather determined by the quality of the provided nitrogen

1 source and the resulting internal allocation patterns. Growth rates were measured halfway
2 through the procedure during a two-fold dilution cycle (**Fig. 1B, Supp. Table S1**). To measure
3 the proteome and transcriptome allocation as a function of the growth rate, we performed
4 label-free proteomics and RNA sequencing (RNA-Seq) analysis of cells from each culture
5 condition (**Methods, Supp. Table S2-S5**).

6 We first asked whether the fission yeast proteome composition differed significantly between
7 the eight growth conditions. Strikingly, ~44% of the 2045 proteins robustly detected in all
8 samples were significantly more variable across conditions than among biological replicates
9 (Holm-adjusted $p_{\text{ANOVA}} < 0.05$). This pervasive level of gene regulation was also apparent at
10 the transcriptome level where ~52% of mRNAs showed significant variability. These results
11 indicate that the composition of the proteome and transcriptome are both strongly affected by
12 conditions that change the growth rate.

13 To investigate this variability further, we used the z-score transformed protein fraction of each
14 gene for hierarchical clustering (**Fig. 2A, Methods**). This treatment enabled normalisation for
15 protein expression levels across the proteome while preserving the variation of each protein
16 between conditions. We defined 10 clusters that revealed two major features of the datasets
17 (**Fig. 2A-C**). First, most clusters showed a clear change in protein expression in one or more
18 conditions (clusters 3-10). Second, the expression of several proteins was not strictly
19 condition-specific but instead showed a coordinated linear increase with growth rate (clusters
20 1-2). Interestingly, the total baseline expression of the condition-specific clusters was
21 positively (clusters 3, 4, 6, 10), or negatively (clusters 5, 7, 8, 9) correlated with the growth
22 rate. Apart from cluster 6, clusters were enriched for defined functional categories, indicating
23 that the shifting balance between condition-specific regulation and growth rate regulation may
24 have physiological consequences related to the enriched functions (**Fig. 2A, Supp. Fig. S2.1**).

25 Both modes of regulation were also apparent in the transcriptome data for coding and non-
26 coding RNA (ncRNA) (**Fig. 2C, Supp. Figs. S2.2-S2.3**). Interestingly, most ncRNAs showed
27 clear and reproducible condition-specific expression between replicates, suggesting the
28 presence of active regulation, consistent with analyses using different genetic and
29 physiological conditions (**Fig. S2.3**) (Atkinson et al. 2018). To test this hypothesis, we
30 compared the expression patterns of ncRNA from each cluster with the expression of their
31 flanking coding genes (**Supp. Fig. S2.3C-D**). We found that for 4 out of 9 clusters, ncRNA
32 expression patterns were not mirrored by the neighbouring mRNA. This indicates that many
33 ncRNA are subjected to some level of independent regulation. In summary, we find that
34 regulation of gene expression programmes across conditions that affect the growth rate has

1 two components; one which is condition-specific and another which is coordinated with growth
2 rate.

3 **Growth dependent gene expression is an important determinant of the cell protein and**
4 **mRNA composition**

5 We first focused our analysis on the growth-dependent component of fission yeast gene
6 expression. Linear correlations between the expression of individual genes and the growth
7 rate have been observed in several organisms under different types of growth limitation
8 (Brauer et al. 2008; Hui et al. 2015; Metzl-Raz et al. 2017; Peebo et al. 2015; A. Schmidt et
9 al. 2016; Zavřel et al. 2019). Following the terminology used in prokaryotes, we divided
10 proteins and mRNA into three sectors depending on whether they show a growth-dependent
11 component that was positively (R), negatively (P), or not significantly (Q) correlated with the
12 growth rate (Scott et al. 2014; 2010). We used repeated-median linear models to quantify the
13 linear coordination of each protein and mRNA quantity with growth. This model fits a linear
14 dependence in the presence of large numbers of outliers and is therefore robust to the
15 condition-specific component of gene expression (**Methods, Supp. Fig. S2.4, Supp. Table**
16 **S6**).

17 The linear fits generated two useful parameters. First, the slope of the linear regression is a
18 measure of the strength of the dependence of a protein's concentration on the growth rate.
19 Second, its *y*-intercept represents the fraction of the protein numbers that is not directly
20 dependent on growth. Both parameters are directly correlated with expression levels making
21 it difficult to disentangle the strength of the growth-rate-related regulation from an mRNA or
22 protein from its abundance. To take this into account, we developed a normalised measure of
23 growth dependence called FC (**Methods, Supp. Fig. S2.4G-H**). FC values are a combination
24 of the regression slope and *y*-intercept which do not scale with abundance, thereby enabling
25 a direct comparison of the growth-dependence of single genes or groups thereof.

26 Repeated-median linear models captured the growth-dependent component of the 10 clusters
27 from **Fig. 2**, and proteins from the R and P sectors dominated the clusters that were positively
28 and negatively correlated with growth, respectively (**Supp. Fig. S2.5**). Of all the genes
29 detected in the proteome across the eight conditions examined, we found that 24% of proteins
30 and 37% of mRNA belonged to the R sector; similarly, 27% and 21% of the proteins and
31 mRNA belonged to the P sector, respectively. The protein and mRNA of a given gene
32 belonged to the same sector in 51% of the cases (**Fig. 2D**). When they did not, the mRNA of
33 P or R proteins were mostly assigned to the Q sector and vice versa, with only 23 R proteins
34 having P sector mRNA, and 74 P proteins having R sector mRNA, out of the 2077 proteins
35 detected.

1 In quantitative terms, the total proteome mass fraction of the fission yeast R sector ranged
2 between ~20% at zero growth and 55% for the fastest measured growth rate, whereas the
3 mass fraction of the P sector similarly ranged from ~30% to 10% (**Fig. 2E**). The sum of all Q
4 sector proteins was negatively correlated with the growth rate because proteome fractions add
5 up to one by definition. However, none of the individual proteins showed significant correlation
6 with the growth rate. At the mRNA level, the R fraction ranged from 38% to 59% of the total
7 normalised counts, and the P fraction from 19% to 10% (**Fig. 2F**). Thus, during fast growth,
8 over half of the gene expression burden is dedicated to factors that increase in concentration
9 with growth rate and may therefore be limiting. Moreover, the amplitude of the variability in the
10 concentration of fission yeast proteins and mRNA that depend on the growth rate alone is in
11 the order of magnitude of the cut-offs that are commonly used for differential expression
12 analysis. Therefore, differences in growth rate are important factors that affect interpretation
13 of transcriptomics and proteomics data (Yu et al. 2021).

14 **R sector proteins participate in all steps of the protein synthesis process**

15 We next queried the cellular processes that had a strong R component and could therefore
16 be either limiting for growth or regulated by it. We used a curated list of macromolecular
17 complexes spanning most cellular processes and calculated the proportion of each complex
18 subunit that was growth rate-dependent in each category (**Fig. 3A, Supp. Table S7**) (Gene
19 Ontology Consortium 2019; Lock et al. 2019). As observed in prokaryotes and budding yeast,
20 the top 4 categories relying the most on R proteins belonged to a single process: the synthesis
21 of proteins (**Fig. 3AB**). Strikingly, R complexes were found at every single step of protein
22 synthesis: the transcription of rRNAs and tRNAs and their processing, assembly and post-
23 translational modification of the ribosome, and initiation and termination of translation (**Fig.**
24 **3B**). Interestingly, expression of the chromatin-modifying complexes NuA4 and Ino80 were
25 part of the R sector (**Fig. 3C**), suggesting they may be involved in ribosome biogenesis in
26 fission yeast as has been proposed for NuA4 in budding yeast (Uprety, Sen, and Bhaumik
27 2015). Alternatively, these results could indicate that the chromatin structure and levels of
28 histone modification may be limiting for growth.

29 The overall correlation between growth and the factors involved in protein synthesis had a
30 notable exception. Although RNA polymerase (RNAP) I and specific subunits of RNAPIII were
31 part of the R sector, RNA polymerase II specific subunits were not significantly correlated with
32 growth rate (**Fig. 3B-D**). Therefore, the number of RNAP II complexes is unlikely to be a
33 limiting step in protein production during growth. Interestingly, RNAP II numbers were found
34 to be limiting for the scaling of gene expression to cell size, indicating that coordination of gene

1 expression to cell size and growth rate follow different mechanisms (Padovan-Merhar et al.
2 2015; Sun et al. 2020).

3 **The stoichiometry of translation complexes changes with the growth rate**

4 Differences in FC values between protein complexes indicate that their relative levels or
5 stoichiometry changes with the growth rate. We hypothesised that these variations could
6 provide mechanistic insights into the functioning of these complexes. To investigate this in the
7 context of protein translation, we analysed three non-overlapping subclasses of translation
8 proteins: the ribosomal proteins (RP), the ribosome biogenesis regulon (RiBi), and the
9 translation initiation, elongation and termination factors (IET) (**Methods, Supp. Table S8**).
10 The RiBi and IET classes had similar FC values, whereas the trendline for RPs was
11 significantly steeper (**Fig. 4A, Supp. Fig. S4.1A**). As a result, the ratios between IET and RPs,
12 and between RiBi proteins and RPs were higher at slow growth (**Fig. 4B**). These results
13 suggest that ribosome biogenesis may become more efficient with increasing growth rates as
14 the ratio RiBi/RP diminishes. Alternatively, a fraction of IET and RiBi proteins larger than of
15 RPs could be held in reserve at slower growth (Metzl-Raz et al. 2017). The relative
16 abundances in EMM of IET:RiBi:RP were approximately 4:1:8 for the proteome mass fractions
17 and 5:4:64 for the transcriptome RPKMs (**Fig. 4A-B**). This confirms earlier observations that
18 the burden on transcription for RP synthesis is higher than for the rest of the proteome
19 (Marguerat et al. 2012; M. W. Schmidt et al. 2007). The growth laws for the initiation and
20 elongation factors were almost identical to each other, suggesting constant stoichiometry with
21 the growth rate (**Supp. Fig. S4.1B-C**). Within the IET category, elongation factors were about
22 three times as abundant as initiation factors, and about fifty times compared to termination
23 factors (**Supp. Fig. S4.1B-C**). This is in line with biochemical evidence showing that translation
24 initiation is a limiting step for protein synthesis (Aylett and Ban 2017). Taken together, we have
25 shown how the growth law can inform on the regulation of gene expression through changes
26 in the stoichiometry of factors with the growth rate.

27 Furthermore, the large burden of RPs during fast growth resulted from the coordinated growth-
28 related expression of most individual RPs and from a growth dependence component steeper
29 than that of IET and RiBi (**Fig. 4C**). This indicates that the aggregate burden of RPs results
30 from coordinated regulation at the level of single genes (Petibon et al. 2020). The IET and RiBi
31 categories also contained more proteins that were assigned to the P- and Q-sectors, and/or
32 whose expression data was not well explained by the robust model due to significant condition-
33 dependent expression (**Supp. Fig. S4.2**). For instance, the initiation factor eIF3E was present
34 in sub-stoichiometric amounts relative to eIF3A. Interestingly eIF3E has been shown to
35 selectively regulate the translation of transcripts coding for metabolic enzymes (Shah et al.
36 2016).

1 Principles of proteome allocation are often conserved in prokaryotes and eukaryotes despite
2 significant mechanistic differences in the way genes are transcribed and translated (Dai and
3 Zhu 2020). Therefore, we thought to compare our findings in fission yeast with published
4 datasets from the budding yeast *S. cerevisiae* and the bacterium *E. coli* (A. Schmidt et al.
5 2016; Metzl-Raz et al. 2017). We reanalysed the proteomics data for *E. coli* cells growing at
6 different rates in a series of environmental conditions and extracted the growth law parameters
7 for translational proteins (**Methods, Supp. Table S9**) (A. Schmidt et al. 2016). For *S.*
8 *cerevisiae*, we used growth law parameters of ribosomal proteins published elsewhere (Metzl-
9 Raz et al. 2017). We found that *E. coli* could sustain a given growth rate with a smaller fraction
10 of RPs than both yeasts (note the smaller slope, **Fig. 4D**). This suggests that the effective
11 translation rate in the yeasts is lower than that of *E. coli*. Among the two yeasts, fission yeast
12 used its RPs significantly more efficiently than the budding yeast trendline, but the effect could
13 not be assigned to a significant difference in either the slope or the intercept parameter
14 specifically. Next, we asked whether the changes in stoichiometry of translational proteins
15 during slow growth were conserved in *E. coli*. Again, both the IET/RP and RiBi/RP ratios were
16 higher during slower growth (**Supp. Fig. S4.3A-B**), because the individual RPs had steeper
17 growth laws (**Supp. Fig. S4.3C**). A steeper growth law of RPs than that of elongation factors
18 was recently predicted by a model of *E. coli* that minimised the total expression cost (Hu et al.
19 2020). Our results indicate that allocation strategies are conserved even though protein
20 production differs mechanistically between the two kingdoms.

21 **P sector proteins are part of the core environmental stress response programme**

22 To complement our analysis of the R sector, we next examined fission yeast proteins from the
23 P sector, i.e., proteins with a negative growth-dependent component. In contrast to the R
24 sector clusters 1 and 2, we could not identify P sector clusters whose expression could be
25 explained exclusively by a negative growth rate correlation (**Fig. 1A-C**). This indicates that
26 proteins with a strong P component are also often regulated in response to specific nitrogen
27 sources. Moreover, the growth component for P proteins was less significant overall than for
28 R proteins (**Supp. Fig. S4.4A-B**). These results suggest that regulation of the R and P sectors
29 may differ mechanistically.

30 Unlike R proteins, which are mostly involved in protein production, P proteins belonged to a
31 diverse set of complexes participating in a large array of functions (**Fig. 3A**). As individual
32 proteins, they showed weaker correlations than R sector complexes (**Supp. Fig. S4.4C-D**).
33 To analyse whether this diverse set of P proteins was participating in a common higher-level
34 functional programme we analysed the fission yeast GO-slims alongside 21 lists covering
35 fission yeast physiology and environmental responses (**Fig. 4E, Supp. Fig. S4.5A**) (Mata et
36 al. 2002; D. Chen et al. 2003; Rustici et al. 2004; Marguerat et al. 2012; Rallis, Codlin, and

1 Bähler 2013; Saint et al. 2019; Kamrad et al. 2020). Functional classes with strong P-sector
2 components included vacuole biology, endosome and phagosome, transport and genes
3 induced in the adaptation to nitrogen removal, and/or after treatment with caffeine and
4 rapamycin. The latter two classes, which had the strongest response, are thought to be
5 controlled by TORC1 (Mata et al. 2002; Rallis, Codlin, and Bähler 2013). This suggests that
6 nitrogen sources supporting slower growth rates trigger a form of metabolic stress response.
7 Accordingly, the total expression of the fission yeast core environmental stress response
8 programme upregulated genes (CESR up) was negatively correlated with the growth rate (**Fig.**
9 **4F**). This stress module comprises genes induced in response to a wide range of
10 environmental and genetic perturbations (D. Chen et al. 2003; Pancaldi, Schubert, and Bähler
11 2010). Conversely, genes downregulated as part of the CESR response (CESR down, also
12 called growth module) belonged to the R sector (**Fig. 4F-G, Supp. Fig. S4.5B**). This finding
13 validates the longstanding hypothesis that the balanced expression of the fission yeast stress
14 response is quantitatively connected with the growth rate (López-Maury, Marguerat, and Bähler
15 2008). Additionally, P proteins were enriched for factors regulated during the S phases of the
16 cell cycle, which is consistent with evidence that the cell-cycle phase length differs between
17 nitrogen sources, in particular growth on Trp (**Fig. 4E and Supp. Fig. S4.5C-D**) (Carlson et
18 al. 1999; Rustici et al. 2004).

19 Notably, the functional classes involved in metabolism were not strongly negatively correlated
20 with the growth rate (**Fig. 4E**), and the fission yeast P sector was only marginally enriched in
21 proteins involved in central and energy metabolism (**Supp. Fig. 4.6**). This contrasts with
22 previous data from *E. coli* and *S. cerevisiae* where metabolic genes have been reported to be
23 important components of the P sector (Hui et al. 2015; A. Schmidt et al. 2016; Metzl-Raz et
24 al. 2017). However, when considered globally, the sum of protein mass fractions dedicated to
25 metabolic enzymes was clearly anti-correlated with growth in fission yeast, ranging from ~70%
26 of the proteome in poor nitrogen sources to ~55% in the fastest media (**Fig. 5A**). This indicates
27 that in our system which does not rely on titration of a limiting nutrient to modulate the growth
28 rate, the total protein burden on metabolism is linked to the growth rate, whereas allocation to
29 specific enzymes is not. Therefore, the global anti-correlation of metabolic enzymes with
30 growth rate observed in our data may be a manifestation of the trade-off between metabolism
31 and translation, and not the result of the direct quantitative regulation of metabolic enzymes
32 expression with the growth rate.

33 **The burden of specific metabolic pathways is principally condition-dependent**

34 On top of the growth-dependent components, many fission yeast proteins show clear
35 condition-specific gene regulation (**Fig. 2A-C**, clusters 3-10). Functional analysis indicated an

1 enrichment of these genes for functions related to metabolism. This is consistent with the
2 adoption of distinct metabolic allocation strategies in response to growth with different nitrogen
3 sources (Alam et al. 2016; Mülleter et al. 2016). We classified metabolic genes into six non-
4 overlapping classes based on the following GO terms: canonical glycolysis (GO:0061621),
5 generation of precursors and energy (GO:0006091), cellular amino acid metabolic process
6 (GO:0006520, which includes the interconversion of ammonium, glutamate, and glutamine),
7 lipid metabolic process (GO:0006629), vitamin metabolic process (GO:0006766), and all other
8 metabolic pathways (including transport of metabolites) (**Fig. 5B**, **Supp. Fig. S5.1**, **Supp.**
9 **Table S10**). To avoid overestimating the burden of gene expression by double-counting genes
10 assigned to multiple terms, each protein was assigned only to the first of these GO-terms it
11 was annotated with. The relative allocation to each class was condition-specific, indicating that
12 metabolic states rely differentially on specific pathways (**Fig. 5B**). We note that similar growth
13 rates can be supported by different allocation strategies, as in the case of the Trp and Gly
14 containing media in which cells channelled resources preferentially towards glycolysis (Trp)
15 or amino acid metabolism (Gly) (**Fig. 5B**, **Supp. Fig. S5.1**). The growth-related components
16 of those categories were weak, except for the vitamin metabolism proteins which belonged to
17 the R sector and the precursor/energy proteins that showed a significant P component (see
18 below, **Supp. Fig. S5.1**). Most coenzymes are stable molecules synthesised only as much as
19 necessary to support growth (Hartl et al. 2017). The strong positive correlation of vitamin
20 metabolism expression with growth rate suggests that cells also minimise the translation
21 burden of vitamin metabolic enzymes. In summary expression of metabolic enzymes in our
22 system, although connected to the growth rate, is mainly condition- and pathway-specific.

23 We next took a closer look at the energy metabolism pathways and their negative correlation
24 with the growth rate. Nutrient quality, cell growth, and energy metabolism are intimately
25 connected. The generation of ATP through fermentation is often favoured in conditions that
26 support faster growth whereas slow-growing cells in limiting conditions tend to switch to
27 respiratory metabolism (Heiden, Cantley, and Thompson 2009; Shimizu and Matsuoka 2018).
28 Therefore, we asked whether protein allocation to either energy metabolism pathway was
29 correlated with the nitrogen sources used and/or growth rate. To this end, we split the non-
30 glycolytic generation of precursors and energy category into the fermentative enzymes
31 pyruvate decarboxylase (Pdc101) and alcohol dehydrogenase (Adh1), and the respiration
32 process into tricarboxylic acid cycle (TCA, GO: 0006099) and oxidative phosphorylation
33 (OXPHOS, GO:0006119) enzymes (**Fig. 5C**, **Supp. Fig. S5.2**). Surprisingly, none of the
34 categories were consistently correlated with the growth rate. Instead, condition-specific
35 expression was dominant, and a clear repression of all OXPHOS complexes upon growth on
36 serine was observed (**Supp. Fig. S5.3**). A recent report showed that serine catabolism

1 generates high levels of reactive oxygen species (ROS) in *S. pombe*, suggesting that
2 respiration may be repressed upon growth on serine to avoid a further increase in ROS (Kanou
3 et al. 2020). Notably, expression of the fermentative enzymes Adh1 and Pdc101, although
4 variable between conditions, was consistently higher than the total expression of the
5 respiratory enzymes. Moreover, respiratory enzymes were not induced in nitrogen sources
6 supporting slow growth. Taken together, the expression balance between fermentation and
7 respiratory enzymes was not quantitatively connected to the growth rate, but depended on the
8 nutrient properties.

9 To complement this analysis, we searched for condition-specific patterns of protein expression
10 that were not related to the growth rate in our proteomics dataset using principal component
11 analysis (PCA) (**Supp. Fig. S5.4**). The first principal component (PC1) explained 29% of the
12 total variance and split the culture conditions in two irrespective of the growth rate with Trp
13 (W), Phe (F), Ser (S), and Pro (P) in one group (from here on termed the WFSP media) and
14 Gly (G), Ile (I), Glu (E) and Amm in the other (**Fig. 5D**). Strikingly 24% (495/2045) of proteins
15 had more than 50% of their variance explained by PC1. We defined two large classes of
16 protein based on their response to this component: i) WFSP+ consisting of 275 proteins that
17 were positively correlated with PC1 and therefore induced in the WFSP media; ii) WFSP-
18 characterised by 220 proteins with expression negatively correlated with PC1 and therefore
19 repressed in the WFSP media (**Supp. Table S11**). Interestingly, no single principal component
20 was dominated by growth rate correlation (**Supp. Fig. S5.4E**), reinforcing the point that
21 nutrient-specific and growth-dependent components of gene expression coexist for many
22 proteins.

23 Glycolytic and NAD-dependent enzymes were the two major classes of proteins
24 overrepresented in the WFSP lists. First, most glycolytic enzymes belonged to one of the two
25 WFSP classes (**Fig. 5E-F, Supp. Fig. S5.5**). These enzymes were highly expressed across
26 conditions, amounting to ~15%–30% of the total proteome mass (**Fig. 5B, Supp. Fig. S5.1**).
27 Therefore, the total gene expression burden of cellular metabolism across the WFSP
28 conditions was heavily affected by the abundance of a small number of enzymes. Second, the
29 two enzymes glyceraldehyde-3-phosphate (G3P) dehydrogenase Tdh1 and alcohol
30 dehydrogenase Adh1 were assigned to opposing WFSP lists, and the ratio of Adh1/Tdh1
31 expression was highly elevated in the WFSP conditions (**Fig. 5F-G**). Fermentation of a single
32 molecule of glucose generates two molecules of ethanol and carbon dioxide. During the
33 process, Tdh1 reduces two NAD⁺ molecules and Adh1 oxidises two NADH molecules.
34 Therefore, the elevated Adh1/Tdh1 balance exerts a pressure on the NAD⁺/NADH equilibrium
35 towards the NAD⁺ side. The induction of Adh1 and repression of Tdh1 proteins may be a
36 controlled response to maintain homeostasis under disruptions to the NAD⁺/NADH redox

1 balance. This way, differential resource allocation towards the NAD-cycling glycolytic–
2 fermentation pathway may indicate that the metabolic rewiring invoked by the WFSP nitrogen
3 sources could result from changes in the cell redox balance.

4 To follow up on this observation, we further investigated the burden of NAD-dependent
5 pathways. NADH is oxidised by NADH dehydrogenases that are situated in the inner
6 mitochondrial membrane; the enzyme transfers two electrons per NADH molecule to the
7 electron transport chain to power ATP synthesis. On the other hand, NAD⁺ is reduced several
8 times during each iteration of the TCA cycle by the α -ketoglutarate (α KG) dehydrogenase
9 complex (KGDHC), the isocitrate dehydrogenase (IDH) complex, and the malic enzymes.
10 Fission yeast is thought to have two separate NADH dehydrogenase enzymes, Ndi1 and
11 Nde1, with the NAD-binding domain of Ndi1 facing the mitochondrion and Nde1 facing the
12 cytosol. We examined the expression burden of these enzymes in our data and found that,
13 although neither belonged to one of the WFSP lists, the ratio of Nde1/Ndi1 expression was
14 strongly elevated in the WFSP conditions (Fig. 5H, Supp. Fig. S5.6). The IDH complex
15 comprises the two subunits Idh1 and Idh2, and KGDHC consists of four subunits: Kgd1, Kgd2,
16 Ymr31, and Dld1, the latter being part of multiple complexes. Dld1 and Idh2 were part of the
17 WFSP+ class, unlike any of the other subunits. As above, the ratio of protein abundances for
18 Dld1/Kgd1 and Idh2/Idh1 were elevated in the WFSP conditions (Fig. 5I–J, Supp. Fig. S5.6).
19 Therefore, the response to the WFSP nitrogen sources altered the stoichiometry of NAD-
20 dependent enzymatic complexes.

21 Importantly, these signatures were not detected in our transcriptomics data, suggesting a role
22 for post-transcriptional regulation. In line with this, ubiquitin and its related pathways, as well
23 as the translation factors eIF3e and eIF5A, showed strong WFSP patterns suggesting a role
24 for protein stability (Supp. Fig. S2.4E, Supp. Fig. S4.2B–D, Supp. Table S11). In summary,
25 we identified two distinct cellular states that differed in the expression of enzymes involved in
26 fermentation and the cell's redox balance that were not correlated with the growth rate.

27 **Correcting for growth-rate dependence revealed additional transcriptional signatures
28 of growth on single amino acid sources**

29 Defining the heterogeneity of metabolic states is key to a mechanistic understanding of cell
30 population evolution, but this requires disentangling the gene signatures that depend on the
31 growth rate from those that are purely nutrient specific. Our dataset has the unique capacity
32 to achieve this. We performed differential expression analysis on our RNA-Seq dataset, by
33 comparing each growth condition to a reference transcriptome obtained via averaging all the
34 conditions, and corrected for the growth-dependent component of gene expression
35 (**Methods**). We defined 10 signatures (termed R1–R10) by clustering the log₂-transformed

1 fold change ratios with respect to the synthetic reference of all genes that were significantly
2 enriched in at least one condition (**Fig. 6A, Supp. Fig. S6.1, Supp. Table S12**).

3 The 10 signatures covered the differential expression of 2269 genes in total, representing 44%
4 of the fission yeast transcriptome. Five signatures (R3, R4, R7, R8, and R9) were also visible
5 at the proteome level (**Fig. 6B**). About 69% of the mRNA present in the transcriptomic
6 signatures were quantified in at least one condition in the proteome and ~40% were detected
7 in all conditions, indicating that this relatively limited agreement was not due to the lower
8 coverage of the proteomics data.

9 We next performed functional enrichment analyses of the transcriptomics clusters (**Methods**),
10 using Gene Ontology annotations (Gene Ontology Consortium 2019; Lock et al. 2019).
11 Broader functional categories were captured using GO-slim analysis (**Fig. 6C**), and specific
12 pathways using terms from the biological_process ontology with at most 50 annotations
13 (**Supp. Fig. S6.2**). In agreement with our observation that respiratory genes were repressed
14 in Ser medium, the Ser repressed cluster R4 was strongly enriched for genes related to
15 mitochondrial metabolism. Additionally, genes from the Ser induced cluster R8 were enriched
16 for iron ion homeostasis. Both parts of the Ser response contained oxidoreductases, which is
17 compatible with the recently reported high levels of ROS generated by serine catabolism
18 (Kanou et al. 2020). The Trp repressed cluster R3 was enriched for genes related to amino
19 acid metabolism, again suggesting that the slow growth sustained by the Trp medium was not
20 due to any additional burden of disrupted amino acid synthesis. The smaller cluster R9 was
21 enriched for genes related to pheromone activity (M-factor precursors), signalling, and the
22 induction of meiosis (**Supp. Fig. S6.2**). Interestingly, the signature expression across
23 conditions for these genes (induced in Trp, Phe, Pro, and Glu containing media) mirrored that
24 of Mae2 (**Supp. Fig. S2.4F**), which removes excess carbon from the TCA cycle. As meiosis
25 is usually induced by nitrogen starvation (Petersen and Russell 2016), this result suggests
26 that the state of central carbon metabolism may also play a role in the meiotic transition, as
27 (elemental) nitrogen was abundant in all growth media used. Altogether, we identified a rich
28 set of metabolic signatures that were not dependent on the growth rate, but exclusively reflect
29 changes in external nutrients.

30 CONCLUSIONS

31 In this study we quantified the proteome and transcriptome of the fission yeast *S. pombe*
32 grown in eight defined media that affect the growth rate. Each medium contained a single
33 nonlimiting source of nitrogen, such that variations in gene expression were determined by
34 system-level resource allocation and not by the response of a single pathway to the titration
35 of a limiting nutrient. This set up is in contrast to other studies which relied on a specific limiting

1 nutrient to perturb resource allocation while affecting the growth rate (Brauer et al. 2008; Hui
2 et al. 2015), or leaving it constant (Yu et al. 2020) .

3 Using this orthogonal approach, we propose a model in which shifts in resource allocation
4 trigger two layers of gene expression regulation. The first layer consists of gene expression
5 that is significantly correlated with growth rate and the second is condition-specific depending
6 solely on nutrients. Many proteins and mRNAs showed a combination of both layers of
7 regulation. This suggests that condition-specific responses occur on top of a global level gene
8 regulation that is coordinated with the growth rate (Shahrezaei and Marguerat 2015).
9 Importantly, the global layer of regulation discussed here affects relative abundances of
10 proteins and of mRNAs, and is distinct from the scaling of gene expression to the growth rate
11 which ensures constant biomolecule concentrations (Chávez et al. 2016). The mechanisms
12 behind the observation that a large number of mRNA and proteins show some level of global
13 scaling with the growth rate are not entirely clear. It could be related to the fact that expression
14 of the protein production machinery itself increases with the growth rate and to changes in
15 levels of TOR signalling for instance (see below). This could result in different cellular states
16 that feedback globally on gene expression (Keren et al. 2013). It is of note that the growth-
17 rate-dependent component defined in this study might in some cases complicate the
18 interpretation of condition-specific responses and should then be taken into account (Pancaldi,
19 Schubert, and Bähler 2010; Yu et al. 2021).

20 Eukaryotic growth-rate-related gene expression depends to some extent on the TORC1 axis
21 of gene regulation, which is widely conserved across eukaryotes (Weisman 2016; González
22 and Hall 2017; Morozumi and Shiozaki 2021). TORC1 activity is affected by a variety of
23 stressors including nutrient starvation. Upstream of TORC1, the adenosine monophosphate
24 kinase AMPK has been proposed to mediate the response to nitrogen starvation, and
25 intriguingly, the two complexes can inhibit each other (Davie, Forte, and Petersen 2015; Ling
26 et al. 2020). Downstream, the TORC1 pathway is a key regulator of the balance between the
27 stress and growth modules (López-Maury, Marguerat, and Bähler 2008; Rallis, Codlin, and
28 Bähler 2013; Rallis et al. 2014), with targets including eukaryotic initiation factor 2 subunit
29 alpha (eIF2 α) (Valbuena, Rozalén, and Moreno 2012), the SAGA complex (Laboucarié et al.
30 2017), and the rate of fermentation through Greatwall and PP2A B^{555} (Watanabe et al. 2019).
31 These questions are often studied during adaptation to changing conditions and our system
32 using continuous culture in turbidostats provides an attractive set up for future studies of the
33 mechanisms that maintain the stress vs growth gene expression balance in steady-state
34 conditions.

1 We found that known chromatin modifiers belonged to the R-sector. This is intriguing as
2 expression of histones themselves were not dependent on the growth rate (**Supp. Table S6**).
3 This may suggest that number of histones modifying enzymes and levels of modifications are
4 rate limiting for transcription, or alternatively mediate an orthogonal function such as signalling
5 the cell metabolic state through covalent protein modifications (Mellor 2016; Figlia, Willnow,
6 and Teleman 2020; Morgan and Shilatifard 2020). This illustrates the intricate relationship of
7 chromatin structure with the cell metabolism. Moreover, we found that RNAPII expression was
8 not increasing with the growth rate suggesting that, unlike for gene expression scaling to cell
9 size, its numbers are not limiting for the rate of growth (Padovan-Merhar et al. 2015; Sun et
10 al. 2020). Yet, maintaining constant mRNA concentrations requires synthesis or degradation
11 rates to adjust to cell growth. Therefore, other mechanisms such as transcription elongation
12 or mRNA decay rates are likely to be modulated with the growth rate as suggested in budding
13 yeast (Chávez et al. 2016).

14 Discussing protein allocation in term of factors limiting for growth relies on the assumption that
15 expression of all proteins is optimised for growth in any given condition. Recent evidence has
16 challenged this view and has suggested that significant parts of *E. coli* (Valgepea et al. 2013;
17 Peebo et al. 2015; Mori et al. 2017) and budding yeast (Metzl-Raz et al. 2017; Yu et al. 2020)
18 gene expression are not immediately required for sustaining the growth rate and are instead
19 held in reserve. This reserve pool of protein could support cell adaption to sudden
20 environmental changes. It has furthermore been suggested that central carbon metabolism
21 has a large reserve capacity, suggesting that many enzymes may also not be utilised solely
22 to maximise metabolic fluxes (O'Brien, Utrilla, and Palsson 2016; Christodoulou et al. 2018;
23 Yu et al. 2020). In this study, whereas several nutrient-specific regulatory programmes were
24 detected in both the transcriptome and the proteome, such as specific responses to Ser and
25 Trp, this was not true for the WFSP pattern and other transcriptomics signatures (**Figs. 5 and**
26 **6**). This disconnect could means that metabolic pathways are differentially buffered through
27 protein levels and stability which could in turn be interpreted in term of reserve capacity. A
28 better understanding of post-transcriptional regulation in fission yeast will be important to fully
29 understand what causes the high translational burden of metabolism.

30 We found that expression of metabolic enzymes was strongly condition-specific and only
31 marginally anti-correlated with the growth-rate. This condition-specific regulation represented
32 a large change in the gene expression burden, driven by glycolytic proteins and enzymes and
33 complexes relying on NAD turnover. Interestingly, this large variation in expression burden of
34 the carbon metabolism resulted from changes in nitrogen source and occurred in the presence
35 of abundant external glucose. This highlights the fact that metabolic adaptation to external
36 condition is pervasive not only in term of fluxes but also in term of gene expression burden.

1 The catabolism of the backbones of the amino acids used as nitrogen sources could provide
2 a link between nitrogen and carbon metabolism in our system. Our data provide a rich
3 resource to constrain future genome-scale models of fission yeast that integrate metabolism
4 and gene expression, which will allow testing this hypothesis (O'Brien et al. 2013; Sánchez et
5 al. 2017; Y. Chen et al. 2020).

6 An improved understanding of the fundamental principles behind cellular growth and the
7 physiological and translational burden of metabolism across evolutionarily diverse biological
8 systems would influence a wide range of research areas such as microbiology, synthetic
9 biology, and cancer research. Cellular models of growth should integrate strategies used by a
10 variety of organisms under a wide range of conditions, in order to identify common principles.
11 Beyond its contribution to our understanding of gene regulation, this work will support future
12 experimental and modelling efforts aimed at defining the nature of the trade-offs involved in
13 growth, stress resistance, and metabolism across the tree of life.

14 **ACKNOWLEDGEMENTS**

15 We would like to thank Xi-Ming Sun, Lucie Martin, Wenhao Tang, Benjamin Heineike, Jürg
16 Bähler, Juan Mata, and Stephan Kamrad for critical reading of the manuscript, as well as
17 Pranas Grigaitis, Eunice van Pelt-Kleinjan, and the Shahrezaei, Marguerat and Ralser labs for
18 discussion and feedback. We would like to thank the MRC LMS Genomics facility for help with
19 sequencing. I.T.K. was supported by the Wellcome Trust [203968/Z/16/Z]. F.B. received
20 financial support from Leverhulme Research Project Grant (RPG-2014-408) awarded to S.M.
21 and V.S. V.S. is supported by the EPSRC Centre for Mathematics of Precision Healthcare
22 (EP/N014529/1). A.M.S., M.S., H.K., and S.M. are supported by the UK Medical Research
23 Council. Proteomics data are deposited in PRIDE (pending) and RNA-seq data in
24 ArrayExpress (pending). For the purpose of open access, the authors have applied a CC BY
25 public copyright licence to any Author Accepted Manuscript version arising from this
26 submission.

27

1 REFERENCES

2 Alam, Mohammad Tauqeer, Aleksei Zelezniak, Michael Mülleder, Pavel Shliaha, Roland Schwarz,
3 Floriana Capuano, Jakob Vowinckel, et al. 2016. 'The Metabolic Background Is a Global
4 Player in *Saccharomyces* Gene Expression Epistasis'. *Nature Microbiology* 1 (February):
5 15030. <https://doi.org/10.1038/nmicrobiol.2015.30>.

6 Anders, Simon, Paul Theodor Pyl, and Wolfgang Huber. 2015. 'HTSeq--a Python Framework to Work
7 with High-Throughput Sequencing Data'. *Bioinformatics (Oxford, England)* 31 (2): 166–69.
8 <https://doi.org/10.1093/bioinformatics/btu638>.

9 Atkinson, Sophie R., Samuel Marguerat, Danny A. Bitton, Maria Rodríguez-López, Charalampos Rallis,
10 Jean-François Lemay, Cristina Cobal, et al. 2018. 'Long Noncoding RNA Repertoire and
11 Targeting by Nuclear Exosome, Cytoplasmic Exonuclease, and RNAi in Fission Yeast'. *RNA*
12 (New York, N.Y.) 24 (9): 1195–1213. <https://doi.org/10.1261/rna.065524.118>.

13 Aylett, Christopher H. S., and Nenad Ban. 2017. 'Eukaryotic Aspects of Translation Initiation Brought
14 into Focus'. *Philosophical Transactions of the Royal Society of London. Series B, Biological
15 Sciences* 372 (1716). <https://doi.org/10.1098/rstb.2016.0186>.

16 Basan, Markus, Sheng Hui, Hiroyuki Okano, Zhongge Zhang, Yang Shen, James R. Williamson, and
17 Terence Hwa. 2015. 'Overflow Metabolism in *Escherichia Coli* Results from Efficient
18 Proteome Allocation'. *Nature* 528 (7580): 99–104. <https://doi.org/10.1038/nature15765>.

19 Bertaux, François, Julius von Kügelgen, Samuel Marguerat, and Vahid Shahrezaei. 2020. 'A Bacterial
20 Size Law Revealed by a Coarse-Grained Model of Cell Physiology'. *PLOS Computational
21 Biology* 16 (9): e1008245. <https://doi.org/10.1371/journal.pcbi.1008245>.

22 Björkeroth, Johan, Kate Campbell, Carl Malina, Rosemary Yu, Francesca Di Bartolomeo, and Jens
23 Nielsen. 2020. 'Proteome Reallocation from Amino Acid Biosynthesis to Ribosomes Enables
24 Yeast to Grow Faster in Rich Media'. *Proceedings of the National Academy of Sciences*,
25 August, 201921890. <https://doi.org/10.1073/pnas.1921890117>.

26 Brauer, Matthew J., Curtis Huttenhower, Edoardo M. Airoldi, Rachel Rosenstein, John C. Matese,
27 David Gresham, Viktor M. Boer, Olga G. Troyanskaya, and David Botstein. 2008.
28 'Coordination of Growth Rate, Cell Cycle, Stress Response, and Metabolic Activity in Yeast'.
29 *Molecular Biology of the Cell* 19 (1): 352–67. <https://doi.org/10.1091/mbc.E07-08-0779>.

30 Bremer, Hans, and Patrick P. Dennis. 2008. 'Modulation of Chemical Composition and Other
31 Parameters of the Cell at Different Exponential Growth Rates'. *EcoSal Plus* 3 (1).
32 <https://doi.org/10.1128/ecosal.5.2.3>.

33 Bruggeman, Frank J, Robert Planqué, Douwe Molenaar, and Bas Teusink. 2020. 'Searching for
34 Principles of Microbial Physiology'. *FEMS Microbiology Reviews* 44 (6): 821–44.
35 <https://doi.org/10.1093/femsre/fuaa034>.

36 Campbell, Kate, Lucia Herrera-Dominguez, Clara Correia-Melo, Aleksei Zelezniak, and Markus Ralser.
37 2018. 'Biochemical Principles Enabling Metabolic Cooperativity and Phenotypic
38 Heterogeneity at the Single Cell Level'. *Current Opinion in Systems Biology* 8 (April): 97–108.
39 <https://doi.org/10.1016/j.coisb.2017.12.001>.

40 Carlson, C. R., B. Grallert, T. Stokke, and E. Boye. 1999. 'Regulation of the Start of DNA Replication in
41 *Schizosaccharomyces Pombe*'. *Journal of Cell Science* 112 (6): 939–46.

42 Chávez, Sebastián, José García-Martínez, Lidia Delgado-Ramos, and José E. Pérez-Ortín. 2016. 'The
43 Importance of Controlling mRNA Turnover during Cell Proliferation'. *Current Genetics* 62 (4):
44 701–10. <https://doi.org/10.1007/s00294-016-0594-2>.

45 Chen, Dongrong, W. Mark Toone, Juan Mata, Rachel Lyne, Gavin Burns, Katja Kivinen, Alvis Brazma,
46 Nic Jones, and Jürg Bähler. 2003. 'Global Transcriptional Responses of Fission Yeast to
47 Environmental Stress'. *Molecular Biology of the Cell* 14 (1): 214–29.
48 <https://doi.org/10.1091/mbc.E02-08-0499>.

49 Chen, Yu, Eunice van Pelt-KleinJan, Berdien van Olst, Sieze Douwenga, Sjef Boeren, Herwig
50 Bachmann, Douwe Molenaar, Jens Nielsen, and Bas Teusink. 2020. 'Proteome Constraints

1 Reveal Targets for Improving Microbial Fitness in Nutrient-Rich Environments'. *BioRxiv*,
2 October, 2020.10.15.340554. <https://doi.org/10.1101/2020.10.15.340554>.

3 Christodoulou, Dimitris, Hannes Link, Tobias Fuhrer, Karl Kochanowski, Luca Gerosa, and Uwe Sauer.
4 2018. 'Reserve Flux Capacity in the Pentose Phosphate Pathway Enables *Escherichia coli*'s
5 Rapid Response to Oxidative Stress'. *Cell Systems* 6 (5): 569-578.e7.
6 <https://doi.org/10.1016/j.cels.2018.04.009>.

7 Chubukov, Victor, Luca Gerosa, Karl Kochanowski, and Uwe Sauer. 2014. 'Coordination of Microbial
8 Metabolism'. *Nature Reviews Microbiology* 12 (5): 327-40.
9 <https://doi.org/10.1038/nrmicro3238>.

10 Cox, Jürgen, Marco Y. Hein, Christian A. Luber, Igor Paron, Nagarjuna Nagaraj, and Matthias Mann.
11 2014. 'Accurate Proteome-Wide Label-Free Quantification by Delayed Normalization and
12 Maximal Peptide Ratio Extraction, Termed MaxLFQ'. *Molecular & Cellular Proteomics* 13 (9):
13 2513-26. <https://doi.org/10.1074/mcp.M113.031591>.

14 Cox, Jürgen, and Matthias Mann. 2008. 'MaxQuant Enables High Peptide Identification Rates,
15 Individualized p.p.b.-Range Mass Accuracies and Proteome-Wide Protein Quantification'.
16 *Nature Biotechnology* 26 (12): 1367-72. <https://doi.org/10.1038/nbt.1511>.

17 Dahal, Sanjeev, Jiao Zhao, and Laurence Yang. 2020. 'Genome-Scale Modeling of Metabolism and
18 Macromolecular Expression and Their Applications'. *Biotechnology and Bioprocess
19 Engineering* 25 (6): 931-43. <https://doi.org/10.1007/s12257-020-0061-2>.

20 Dai, Xiongfeng, and Manlu Zhu. 2020. 'Coupling of Ribosome Synthesis and Translational Capacity
21 with Cell Growth'. *Trends in Biochemical Sciences*, May.
22 <https://doi.org/10.1016/j.tibs.2020.04.010>.

23 Dai, Xiongfeng, Manlu Zhu, Mya Warren, Rohan Balakrishnan, Vadim Patsalo, Hiroyuki Okano, James
24 R. Williamson, Kurt Fredrick, Yi-Ping Wang, and Terence Hwa. 2016. 'Reduction of
25 Translating Ribosomes Enables *Escherichia coli* to Maintain Elongation Rates during Slow
26 Growth'. *Nature Microbiology* 2 (2): nmicrobiol2016231.
27 <https://doi.org/10.1038/nmicrobiol.2016.231>.

28 Davie, Elizabeth, Gabriella M. A. Forte, and Janni Petersen. 2015. 'Nitrogen Regulates AMPK to
29 Control TORC1 Signaling'. *Current Biology* 25 (4): 445-54.
30 <https://doi.org/10.1016/j.cub.2014.12.034>.

31 Ducret, A., I. Van Oostveen, J. K. Eng, J. R. Yates, and R. Aebersold. 1998. 'High Throughput Protein
32 Characterization by Automated Reverse-Phase Chromatography/Electrospray Tandem Mass
33 Spectrometry'. *Protein Science: A Publication of the Protein Society* 7 (3): 706-19.
34 <https://doi.org/10.1002/pro.5560070320>.

35 Fantes, P., and P. Nurse. 1977. 'Control of Cell Size at Division in Fission Yeast by a Growth-
36 Modulated Size Control over Nuclear Division'. *Experimental Cell Research* 107 (2): 377-86.
37 [https://doi.org/10.1016/0014-4827\(77\)90359-7](https://doi.org/10.1016/0014-4827(77)90359-7).

38 Figlia, Gianluca, Philipp Willnow, and Aurelio A. Teleman. 2020. 'Metabolites Regulate Cell Signaling
39 and Growth via Covalent Modification of Proteins'. *Developmental Cell* 54 (2): 156-70.
40 <https://doi.org/10.1016/j.devcel.2020.06.036>.

41 Gene Ontology Consortium. 2019. 'The Gene Ontology Resource: 20 Years and Still GOing Strong'.
42 *Nucleic Acids Research* 47 (D1): D330-38. <https://doi.org/10.1093/nar/gky1055>.

43 Godard, Patrice, Antonio Urrestarazu, Stéphan Vissers, Kevin Kontos, Gianluca Bontempi, Jacques
44 van Helden, and Bruno André. 2007. 'Effect of 21 Different Nitrogen Sources on Global Gene
45 Expression in the Yeast *Saccharomyces cerevisiae*'. *Molecular and Cellular Biology* 27 (8):
46 3065-86. <https://doi.org/10.1128/MCB.01084-06>.

47 Goelzer, Anne, and Vincent Fromion. 2017. 'Resource Allocation in Living Organisms'. *Biochemical
48 Society Transactions*, July, BST20160436. <https://doi.org/10.1042/BST20160436>.

49 Goelzer, Anne, Jan Muntel, Victor Chubukov, Matthieu Jules, Eric Prestel, Rolf Nölker, Mahendra
50 Mariadassou, et al. 2015. 'Quantitative Prediction of Genome-Wide Resource Allocation in

1 Bacteria'. *Metabolic Engineering* 32 (November): 232–43.
2 <https://doi.org/10.1016/j.ymben.2015.10.003>.

3 González, Asier, and Michael N. Hall. 2017. 'Nutrient Sensing and TOR Signaling in Yeast and
4 Mammals'. *The EMBO Journal* 36 (4): 397–408. <https://doi.org/10.15252/embj.201696010>.

5 Groot, Daan H. de, Julia Lischke, Riccardo Muolo, Robert Planqué, Frank J. Bruggeman, and Bas
6 Teusink. 2019. 'The Common Message of Constraint-Based Optimization Approaches:
7 Overflow Metabolism Is Caused by Two Growth-Limiting Constraints'. *Cellular and Molecular
8 Life Sciences*, November. <https://doi.org/10.1007/s00018-019-03380-2>.

9 Hartl, Johannes, Patrick Kiefer, Fabian Meyer, and Julia A. Vorholt. 2017. 'Longevity of Major
10 Coenzymes Allows Minimal de Novo Synthesis in Microorganisms'. *Nature Microbiology* 2
11 (7): 1–9. <https://doi.org/10.1038/nmicrobiol.2017.73>.

12 Heiden, Matthew G. Vander, Lewis C. Cantley, and Craig B. Thompson. 2009. 'Understanding the
13 Warburg Effect: The Metabolic Requirements of Cell Proliferation'. *Science* 324 (5930):
14 1029–33. <https://doi.org/10.1126/science.1160809>.

15 Hoek, Milan JA van, and Roeland MH Merks. 2012. 'Redox Balance Is Key to Explaining Full vs. Partial
16 Switching to Low-Yield Metabolism'. *BMC Systems Biology* 6 (1): 22.
17 <https://doi.org/10.1186/1752-0509-6-22>.

18 Hu, Xiao-Pan, Hugo Dourado, Peter Schubert, and Martin J. Lercher. 2020. 'The Protein Translation
19 Machinery Is Expressed for Maximal Efficiency in Escherichia Coli'. *Nature Communications*
20 11 (1): 5260. <https://doi.org/10.1038/s41467-020-18948-x>.

21 Huber, W., V. J. Carey, R. Gentleman, S. Anders, M. Carlson, B. S. Carvalho, H. C. Bravo, et al. 2015.
22 'Orchestrating High-Throughput Genomic Analysis with Bioconductor'. *Nature Methods* 12
23 (2): 115–21.

24 Hui, Sheng, Josh M. Silverman, Stephen S. Chen, David W. Erickson, Markus Basan, Jilong Wang,
25 Terence Hwa, and James R. Williamson. 2015. 'Quantitative Proteomic Analysis Reveals a
26 Simple Strategy of Global Resource Allocation in Bacteria'. *Molecular Systems Biology* 11:
27 784.

28 Irving, Sophie E., Naznin R. Choudhury, and Rebecca M. Corrigan. 2020. 'The Stringent Response and
29 Physiological Roles of (Pp)PGpp in Bacteria'. *Nature Reviews. Microbiology*, November.
30 <https://doi.org/10.1038/s41579-020-00470-y>.

31 Jun, Suckjoon, Fangwei Si, Rami Pugatch, and Matthew Scott. 2018. 'Fundamental Principles in
32 Bacterial Physiology—History, Recent Progress, and the Future with Focus on Cell Size
33 Control: A Review'. *Reports on Progress in Physics* 81 (5): 056601.
34 <https://doi.org/10.1088/1361-6633/aaa628>.

35 Kamrad, Stephan, Jan Grossbach, Maria Rodríguez-López, Michael Mülleder, StJohn Townsend,
36 Valentina Cappelletti, Gorjan Stojanovski, et al. 2020. 'Pyruvate Kinase Variant of Fission
37 Yeast Tunes Carbon Metabolism, Cell Regulation, Growth and Stress Resistance'. *Molecular
38 Systems Biology* 16 (4): e9270. <https://doi.org/10.1525/msb.20199270>.

39 Kanou, Akihiko, Shinichi Nishimura, Toshitsugu Tabuchi, Akihisa Matsuyama, Minoru Yoshida, Taira
40 Kato, and Hideaki Kakeya. 2020. 'Serine Catabolism Produces ROS, Sensitizes Cells to Actin
41 Dysfunction, and Suppresses Cell Growth in Fission Yeast'. *The Journal of Antibiotics* 73 (8):
42 574–80. <https://doi.org/10.1038/s41429-020-0305-6>.

43 Keren, Leeat, Ora Zackay, Maya Lotan-Pompan, Uri Barenholz, Erez Dekel, Vered Sasson, Guy
44 Aidelberg, et al. 2013. 'Promoters Maintain Their Relative Activity Levels under Different
45 Growth Conditions'. *Molecular Systems Biology* 9 (1): 701.
46 <https://doi.org/10.1038/msb.2013.59>.

47 Kim, Daehwan, Geo Pertea, Cole Trapnell, Harold Pimentel, Ryan Kelley, and Steven L. Salzberg.
48 2013. 'TopHat2: Accurate Alignment of Transcriptomes in the Presence of Insertions,
49 Deletions and Gene Fusions'. *Genome Biology* 14 (4): R36. <https://doi.org/10.1186/gb-2013-14-4-r36>.

1 Klumpp, Stefan, and Terence Hwa. 2014. 'Bacterial Growth: Global Effects on Gene Expression,
2 Growth Feedback and Proteome Partition'. *Current Opinion in Biotechnology*,
3 *Nanobiotechnology • Systems biology*, 28 (August): 96–102.
4 <https://doi.org/10.1016/j.copbio.2014.01.001>.

5 Kohanim, Yael Korem, Dikla Levi, Ghil Jona, Benjamin D. Towbin, Anat Bren, and Uri Alon. 2018. 'A
6 Bacterial Growth Law out of Steady State'. *Cell Reports* 23 (10): 2891–2900.
7 <https://doi.org/10.1016/j.celrep.2018.05.007>.

8 Komsta, Lukasz. 2019. *Mblm: Median-Based Linear Models* (version 0.12.1). <https://CRAN.R-project.org/package=mblm>.

9 Laboucarié, Thomas, Dylane Detilleux, Ricard A. Rodriguez-Mias, Céline Faux, Yves Romeo, Miritा
10 Franz-Wachtel, Karsten Krug, et al. 2017. 'TORC1 and TORC2 Converge to Regulate the SAGA
11 Co-activator in Response to Nutrient Availability'. *EMBO Reports* 18 (12): 2197–2218.
12 <https://doi.org/10.15252/embr.201744942>.

13 Liao, Chen, Andrew E. Blanchard, and Ting Lu. 2017. 'An Integrative Circuit–Host Modelling
14 Framework for Predicting Synthetic Gene Network Behaviours'. *Nature Microbiology*,
15 September, 1. <https://doi.org/10.1038/s41564-017-0022-5>.

16 Ling, Naomi X. Y., Adrian Kaczmarek, Ashfaqul Hoque, Elizabeth Davie, Kevin R. W. Ngoei, Kaitlin R.
17 Morrison, William J. Smiles, et al. 2020. 'MTORC1 Directly Inhibits AMPK to Promote Cell
18 Proliferation under Nutrient Stress'. *Nature Metabolism* 2 (1): 41–49.
19 <https://doi.org/10.1038/s42255-019-0157-1>.

20 Lock, Antonia, Kim Rutherford, Midori A. Harris, Jacqueline Hayles, Stephen G. Oliver, Jürg Bähler,
21 and Valerie Wood. 2019. 'PomBase 2018: User-Driven Reimplementation of the Fission Yeast
22 Database Provides Rapid and Intuitive Access to Diverse, Interconnected Information'.
23 *Nucleic Acids Research* 47 (D1): D821–27. <https://doi.org/10.1093/nar/gky961>.

24 López-Maury, Luis, Samuel Marguerat, and Jürg Bähler. 2008. 'Tuning Gene Expression to Changing
25 Environments: From Rapid Responses to Evolutionary Adaptation'. *Nature Reviews Genetics*
26 9 (8): 583–93. <https://doi.org/10.1038/nrg2398>.

27 Love, Michael I., Wolfgang Huber, and Simon Anders. 2014. 'Moderated Estimation of Fold Change
28 and Dispersion for RNA-Seq Data with DESeq2'. *Genome Biology* 15 (December): 550.
29 <https://doi.org/10.1186/s13059-014-0550-8>.

30 Luengo, Alba, Zhaoqi Li, Dan Y. Gui, Lucas B. Sullivan, Maria Zagorulya, Brian T. Do, Raphael Ferreira,
31 et al. 2020. 'Increased Demand for NAD+ Relative to ATP Drives Aerobic Glycolysis'.
32 *Molecular Cell* 0 (0). <https://doi.org/10.1016/j.molcel.2020.12.012>.

33 Lyne, Rachel, Gavin Burns, Juan Mata, Chris J. Penkett, Gabriella Rustici, Dongrong Chen, Cordelia
34 Langford, David Vetrici, and Jürg Bähler. 2003. 'Whole-Genome Microarrays of Fission Yeast:
35 Characteristics, Accuracy, Reproducibility, and Processing of Array Data'. *BMC Genomics* 4
36 (1): 27. <https://doi.org/10.1186/1471-2164-4-27>.

37 Maitra, Arijit, and Ken A. Dill. 2015. 'Bacterial Growth Laws Reflect the Evolutionary Importance of
38 Energy Efficiency'. *Proceedings of the National Academy of Sciences* 112 (2): 406–11.
39 <https://doi.org/10.1073/pnas.1421138111>.

40 Malecki, Michal, Stephan Kamrad, Markus Ralser, and Jürg Bähler. 2020. 'Mitochondrial Respiration
41 Is Required to Provide Amino Acids during Fermentative Proliferation of Fission Yeast'.
42 *BioRxiv*, February, 2020.02.12.946111. <https://doi.org/10.1101/2020.02.12.946111>.

43 Marguerat, Samuel, Alexander Schmidt, Sandra Codlin, Wei Chen, Ruedi Aebersold, and Jürg Bähler.
44 2012. 'Quantitative Analysis of Fission Yeast Transcriptomes and Proteomes in Proliferating
45 and Quiescent Cells'. *Cell* 151 (3): 671–83. <https://doi.org/10.1016/j.cell.2012.09.019>.

46 Mata, Juan, Rachel Lyne, Gavin Burns, and Jürg Bähler. 2002. 'The Transcriptional Program of
47 Meiosis and Sporulation in Fission Yeast'. *Nature Genetics* 32 (1): 143–47.
48 <https://doi.org/10.1038/ng951>.

1 Mellor, Jane. 2016. 'The Molecular Basis of Metabolic Cycles and Their Relationship to Circadian
2 Rhythms'. *Nature Structural & Molecular Biology* 23 (12): 1035–44.
3 <https://doi.org/10.1038/nsmb.3311>.

4 Metzl-Raz, Eyal, Moshe Kafri, Gilad Yaakov, Ilya Soifer, Yonat Gurvich, and Naama Barkai. 2017.
5 'Principles of Cellular Resource Allocation Revealed by Condition-Dependent Proteome
6 Profiling'. *ELife* 6 (August): e28034. <https://doi.org/10.7554/eLife.28034>.

7 Mitchison, J. M., and K. G. Lark. 1962. 'Incorporation of 3H-Adenine into RNA during the Cell Cycle of
8 Schizosaccharomyces Pombe'. *Experimental Cell Research* 28 (2): 452–55.
9 [https://doi.org/10.1016/0014-4827\(62\)90304-X](https://doi.org/10.1016/0014-4827(62)90304-X).

10 Molenaar, Douwe, Rogier van Berlo, Dick de Ridder, and Bas Teusink. 2009. 'Shifts in Growth
11 Strategies Reflect Tradeoffs in Cellular Economics'. *Molecular Systems Biology* 5 (1): 323.
12 <https://doi.org/10.1038/msb.2009.82>.

13 Morgan, Marc A. J., and Ali Shilatifard. 2020. 'Reevaluating the Roles of Histone-Modifying Enzymes
14 and Their Associated Chromatin Modifications in Transcriptional Regulation'. *Nature
15 Genetics* 52 (12): 1271–81. <https://doi.org/10.1038/s41588-020-00736-4>.

16 Mori, Matteo, Severin Schink, David W. Erickson, Ulrich Gerland, and Terence Hwa. 2017.
17 'Quantifying the Benefit of a Proteome Reserve in Fluctuating Environments'. *Nature
18 Communications* 8 (1): 1225. <https://doi.org/10.1038/s41467-017-01242-8>.

19 Morozumi, Yuichi, and Kazuhiro Shiozaki. 2021. 'Conserved and Divergent Mechanisms That Control
20 TORC1 in Yeasts and Mammals'. *Genes* 12 (1): 88. <https://doi.org/10.3390/genes12010088>.

21 Mülleder, Michael, Enrica Calvani, Mohammad Tauqeer Alam, Richard Kangda Wang, Florian
22 Eckerstorfer, Aleksej Zelezniak, and Markus Ralser. 2016. 'Functional Metabolomics
23 Describes the Yeast Biosynthetic Regulome'. *Cell* 167 (2): 553–565.e12.
24 <https://doi.org/10.1016/j.cell.2016.09.007>.

25 Neidhardt, Frederick C., John L. Ingraham, and Moselio Schaechter. 1990. *Physiology of the Bacterial
26 Cell*. Sunderland, MA: Sinauer Associates.

27 O'Brien, Edward J., Joshua A. Lerman, Roger L. Chang, Daniel R. Hyduke, and Bernhard Ø Palsson.
28 2013. 'Genome-scale Models of Metabolism and Gene Expression Extend and Refine Growth
29 Phenotype Prediction'. *Molecular Systems Biology* 9 (1): 693.
30 <https://doi.org/10.1038/msb.2013.52>.

31 O'Brien, Edward J., Jose Utrilla, and Bernhard O. Palsson. 2016. 'Quantification and Classification of
32 E. Coli Proteome Utilization and Unused Protein Costs across Environments'. *PLOS
33 Computational Biology* 12 (6): e1004998. <https://doi.org/10.1371/journal.pcbi.1004998>.

34 Padovan-Merhar, Olivia, Gautham P. Nair, Andrew G. Biaesch, Andreas Mayer, Steven Scarfone,
35 Shawn W. Foley, Angela R. Wu, L. Stirling Churchman, Abhyudai Singh, and Arjun Raj. 2015.
36 'Single Mammalian Cells Compensate for Differences in Cellular Volume and DNA Copy
37 Number through Independent Global Transcriptional Mechanisms'. *Molecular Cell* 58 (2):
38 339–52. <https://doi.org/10.1016/j.molcel.2015.03.005>.

39 Pancaldi, Vera, Falk Schubert, and Jürg Bähler. 2010. 'Meta-Analysis of Genome Regulation and
40 Expression Variability across Hundreds of Environmental and Genetic Perturbations in
41 Fission Yeast'. *Molecular BioSystems* 6 (3): 543–52. <https://doi.org/10.1039/B913876P>.

42 Pandey, Parth Pratim, and Sanjay Jain. 2016. 'Analytic Derivation of Bacterial Growth Laws from a
43 Simple Model of Intracellular Chemical Dynamics'. *Theory in Biosciences* 135 (3): 121–30.
44 <https://doi.org/10.1007/s12064-016-0227-9>.

45 Paulo, Joao A., Jeremy D. O'Connell, Robert A. Everley, Jonathon O'Brien, Micah A. Gygi, and Steven
46 P. Gygi. 2016. 'Quantitative Mass Spectrometry-Based Multiplexing Compares the
47 Abundance of 5000 S. Cerevisiae Proteins across 10 Carbon Sources'. *Journal of Proteomics*
48 148 (Supplement C): 85–93. <https://doi.org/10.1016/j.jprot.2016.07.005>.

49 Paulo, Joao A., Jeremy D. O'Connell, Aleksandr Gaun, and Steven P. Gygi. 2015. 'Proteome-Wide
50 Quantitative Multiplexed Profiling of Protein Expression: Carbon-Source Dependency in

1 Saccharomyces Cerevisiae'. *Molecular Biology of the Cell* 26 (22): 4063–74.
2 <https://doi.org/10.1091/mbc.E15-07-0499>.

3 Peebo, Karl, Kaspar Valgepea, Andres Maser, Ranno Nahku, Kaarel Adamberg, and Raivo Vilu. 2015.
4 'Proteome Reallocation in Escherichia Coli with Increasing Specific Growth Rate'. *Molecular*
5 *BioSystems* 11 (4): 1184–93. <https://doi.org/10.1039/C4MB00721B>.

6 Petersen, Janni, and Paul Russell. 2016. 'Growth and the Environment of Schizosaccharomyces
7 Pombe'. *Cold Spring Harbor Protocols* 2016 (3): pdb.top079764.
8 <https://doi.org/10.1101/pdb.top079764>.

9 Petibon, Cyrielle, Mustafa Malik Ghulam, Mathieu Catala, and Sherif Abou Elela. 2020. 'Regulation of
10 Ribosomal Protein Genes: An Ordered Anarchy'. *Wiley Interdisciplinary Reviews. RNA*,
11 October, e1632. <https://doi.org/10.1002/wrna.1632>.

12 Rallis, C., S. Codlin, and J. Bähler. 2013. 'TORC1 Signaling Inhibition by Rapamycin and Caffeine Affect
13 Lifespan, Global Gene Expression, and Cell Proliferation of Fission Yeast.' *Aging Cell* 12 (4):
14 563–73. <https://doi.org/10.1111/acel.12080>.

15 Rallis, C., L. López-Maury, T. Georgescu, V. Pancaldi, and J. Bähler. 2014. 'Systematic Screen for
16 Mutants Resistant to TORC1 Inhibition in Fission Yeast Reveals Genes Involved in Cellular
17 Ageing and Growth.' *Biology Open* 3 (2): 161–71. <https://doi.org/10.1242/bio.20147245>.

18 Rustici, Gabriella, Juan Mata, Katja Kivinen, Pietro Lió, Christopher J. Penkett, Gavin Burns,
19 Jacqueline Hayles, Alvis Brazma, Paul Nurse, and Jürg Bähler. 2004. 'Periodic Gene
20 Expression Program of the Fission Yeast Cell Cycle'. *Nature Genetics* 36 (8): 809–17.
21 <https://doi.org/10.1038/ng1377>.

22 Saint, Malika, François Bertaux, Wenhao Tang, Xi-Ming Sun, Laurence Game, Anna Köferle, Jürg
23 Bähler, Vahid Shahrezaei, and Samuel Marguerat. 2019. 'Single-Cell Imaging and RNA
24 Sequencing Reveal Patterns of Gene Expression Heterogeneity during Fission Yeast Growth
25 and Adaptation'. *Nature Microbiology*, February, 1. <https://doi.org/10.1038/s41564-018-0330-4>.

26 Sánchez, Benjamín J., Cheng Zhang, Avlant Nilsson, Petri-Jaan Lahtvee, Eduard J. Kerkhoven, and Jens
27 Nielsen. 2017. 'Improving the Phenotype Predictions of a Yeast Genome-scale Metabolic
28 Model by Incorporating Enzymatic Constraints'. *Molecular Systems Biology* 13 (8): 935.
29 <https://doi.org/10.15252/msb.20167411>.

30 Schaechter, M., O. Maaløe, and N. O. Kjeldgaard. 1958. 'Dependency on Medium and Temperature of
31 Cell Size and Chemical Composition during Balanced Growth of *Salmonella Typhimurium*'.
32 *Journal of General Microbiology* 19 (3): 592–606. <https://doi.org/10.1099/00221287-19-3-592>.

33 Schmidt, Alexander, Karl Kochanowski, Silke Vedelaar, Erik Ahrné, Benjamin Volkmer, Luciano
34 Callipo, Kévin Knoops, Manuel Bauer, Ruedi Aebersold, and Matthias Heinemann. 2016. 'The
35 Quantitative and Condition-Dependent Escherichia Coli Proteome'. *Nature Biotechnology* 34
36 (1): 104–10. <https://doi.org/10.1038/nbt.3418>.

37 Schmidt, Michael W, Andres Houseman, Alexander R Ivanov, and Dieter A Wolf. 2007. 'Comparative
38 Proteomic and Transcriptomic Profiling of the Fission Yeast *Schizosaccharomyces Pombe*'.
39 *Molecular Systems Biology* 3 (1): 79. <https://doi.org/10.1038/msb4100117>.

40 Scott, Matthew, Carl W. Gunderson, Eduard M. Mateescu, Zhongge Zhang, and Terence Hwa. 2010.
41 'Interdependence of Cell Growth and Gene Expression: Origins and Consequences'. *Science*
42 330 (November): 1099–1102. <https://doi.org/10.1126/science.1192588>.

43 Scott, Matthew, Stefan Klumpp, Eduard M. Mateescu, and Terence Hwa. 2014. 'Emergence of
44 Robust Growth Laws from Optimal Regulation of Ribosome Synthesis'. *Molecular Systems
45 Biology* 10 (8): 747. <https://doi.org/10.15252/msb.20145379>.

46 Shah, Meera, Dan Su, Judith S. Scheliga, Tomáš Pluskal, Susanna Boronat, Khatereh
47 Motamedchaboki, Alexandre Rosa Campos, et al. 2016. 'A Transcript-Specific EIF3 Complex
48 Mediates Global Translational Control of Energy Metabolism'. *Cell Reports* 16 (7): 1891–
49 1902. <https://doi.org/10.1016/j.celrep.2016.07.006>.

50

51

1 Shahrezaei, Vahid, and Samuel Marguerat. 2015. 'Connecting Growth with Gene Expression: Of
2 Noise and Numbers'. *Current Opinion in Microbiology*, Environmental microbiology •
3 Extremophiles, 25 (June): 127–35. <https://doi.org/10.1016/j.mib.2015.05.012>.

4 Shimizu, Kazuyuki, and Yu Matsuoka. 2018. 'Regulation of Glycolytic Flux and Overflow Metabolism
5 Depending on the Source of Energy Generation for Energy Demand'. *Biotechnology
6 Advances*, December. <https://doi.org/10.1016/j.biotechadv.2018.12.007>.

7 Siegel, Andrew F. 1982. 'Robust Regression Using Repeated Medians'. *Biometrika* 69 (1): 242–44.
8 <https://doi.org/10.1093/biomet/69.1.242>.

9 Silge, Julia, Fanny Chow, Max Kuhn, and Hadley Wickham. 2021. *Rsample: General Resampling
10 Infrastructure* (version 0.0.9). <https://CRAN.R-project.org/package=rsample>.

11 Spinelli, Jessica B., and Marcia C. Haigis. 2018. 'The Multifaceted Contributions of Mitochondria to
12 Cellular Metabolism'. *Nature Cell Biology* 20 (7): 745–54. <https://doi.org/10.1038/s41556-018-0124-1>.

13 Strimmer, Korbinian. 2008. 'Fdrtool: A Versatile R Package for Estimating Local and Tail Area-Based
14 False Discovery Rates'. *Bioinformatics* 24 (12): 1461–62.
15 <https://doi.org/10.1093/bioinformatics/btn209>.

16 Sun, Xi-Ming, Anthony Bowman, Miles Priestman, Francois Bertaux, Amalia Martinez-Segura,
17 Wenhao Tang, Chad Whilding, Dirk Dormann, Vahid Shahrezaei, and Samuel Marguerat.
18 2020. 'Size-Dependent Increase in RNA Polymerase II Initiation Rates Mediates Gene
19 Expression Scaling with Cell Size'. *Current Biology* 0 (0).
20 <https://doi.org/10.1016/j.cub.2020.01.053>.

21 Szenk, Mariola, Ken A. Dill, and Adam M. R. de Graff. 2017. 'Why Do Fast-Growing Bacteria Enter
22 Overflow Metabolism? Testing the Membrane Real Estate Hypothesis'. *Cell Systems* 5 (2):
23 95–104. <https://doi.org/10.1016/j.cels.2017.06.005>.

24 Takahashi, Chris N., Aaron W. Miller, Felix Ekness, Maitreya J. Dunham, and Eric Klavins. 2015. 'A Low
25 Cost, Customizable Turbidostat for Use in Synthetic Circuit Characterization'. *ACS Synthetic
26 Biology* 4 (1): 32–38. <https://doi.org/10.1021/sb500165g>.

27 Uprety, Bhawana, Rwik Sen, and Sukesh R. Bhaumik. 2015. 'Eaf1p Is Required for Recruitment of
28 NuA4 in Targeting TFIID to the Promoters of the Ribosomal Protein Genes for Transcriptional
29 Initiation In Vivo'. *Molecular and Cellular Biology* 35 (17): 2947–64.
30 <https://doi.org/10.1128/MCB.01524-14>.

31 Valbuena, Noelia, Ana Elisa Rozalén, and Sergio Moreno. 2012. 'Fission Yeast TORC1 Prevents EIF2α
32 Phosphorylation in Response to Nitrogen and Amino Acids via Gcn2 Kinase'. *Journal of Cell
33 Science* 125 (24): 5955–59. <https://doi.org/10.1242/jcs.105395>.

34 Valgepea, Kaspar, Kaarel Adamberg, Andrus Seiman, and Raivo Vilu. 2013. 'Escherichia Coli Achieves
35 Faster Growth by Increasing Catalytic and Translation Rates of Proteins'. *Molecular
36 BioSystems* 9 (9): 2344–58. <https://doi.org/10.1039/C3MB70119K>.

37 Vazquez, Alexei, Qasim K. Beg, Marcio A. deMenezes, Jason Ernst, Ziv Bar-Joseph, Albert-László
38 Barabási, László G. Boros, and Zoltán N. Oltvai. 2008. 'Impact of the Solvent Capacity
39 Constraint on E. Coli Metabolism'. *BMC Systems Biology* 2 (January): 7.
40 <https://doi.org/10.1186/1752-0509-2-7>.

41 Vemuri, G. N., M. A. Eiteman, J. E. McEwen, L. Olsson, and J. Nielsen. 2007. 'Increasing NADH
42 Oxidation Reduces Overflow Metabolism in *Saccharomyces Cerevisiae*'. *Proceedings of the
43 National Academy of Sciences* 104 (7): 2402–7. <https://doi.org/10.1073/pnas.0607469104>.

44 Waldron, C., and F. Lacroute. 1975. 'Effect of Growth Rate on the Amounts of Ribosomal and
45 Transfer Ribonucleic Acids in Yeast.' *Journal of Bacteriology* 122 (3): 855–65.

46 Watanabe, Daisuke, Takuma Kajihara, Yukiko Sugimoto, Kenichi Takagi, Megumi Mizuno, Yan Zhou,
47 Jiawen Chen, et al. 2019. 'Nutrient Signaling via the TORC1-Greatwall-PP2AB55δ Pathway Is
48 Responsible for the High Initial Rates of Alcoholic Fermentation in Sake Yeast Strains of
49 *Saccharomyces Cerevisiae*'. *Applied and Environmental Microbiology* 85 (1).
50 <https://doi.org/10.1128/AEM.02083-18>.

51

1 Weisman, Ronit. 2016. 'Target of Rapamycin (TOR) Regulates Growth in Response to Nutritional
2 Signals'. *Microbiology Spectrum* 4 (5). <https://doi.org/10.1128/microbiolspec.FUNK-0006-2016>.

4 Weiße, Andrea Y., Diego A. Oyarzún, Vincent Danos, and Peter S. Swain. 2015. 'Mechanistic Links
5 between Cellular Trade-Offs, Gene Expression, and Growth'. *Proceedings of the National
6 Academy of Sciences* 112 (9): E1038–47. <https://doi.org/10.1073/pnas.1416533112>.

7 Wickham, Hadley. 2016. *Ggplot2: Elegant Graphics for Data Analysis*. Springer-Verlag New York.
8 <https://ggplot2.tidyverse.org>.

9 Yang, Laurence, James T Yurkovich, Zachary A King, and Bernhard O Palsson. 2018. 'Modeling the
10 Multi-Scale Mechanisms of Macromolecular Resource Allocation'. *Current Opinion in
11 Microbiology, Antimicrobials * Microbial systems biology*, 45 (October): 8–15.
12 <https://doi.org/10.1016/j.mib.2018.01.002>.

13 You, Conghui, Hiroyuki Okano, Sheng Hui, Zhongge Zhang, Minsu Kim, Carl W. Gunderson, Yi-Ping
14 Wang, Peter Lenz, Dalai Yan, and Terence Hwa. 2013. 'Coordination of Bacterial Proteome
15 with Metabolism by Cyclic AMP Signalling.' *Nature* 500 (August): 301–6.
16 <https://doi.org/10.1038/nature12446>.

17 Yu, Rosemary, Kate Campbell, Rui Pereira, Johan Björkeroth, Qi Qi, Egor Vorontsov, Carina Sihlbom,
18 and Jens Nielsen. 2020. 'Nitrogen Limitation Reveals Large Reserves in Metabolic and
19 Translational Capacities of Yeast'. *Nature Communications* 11 (1): 1–12.
20 <https://doi.org/10.1038/s41467-020-15749-0>.

21 Yu, Rosemary, Egor Vorontsov, Carina Sihlbom, and Jens Nielsen. 2021. 'Quantifying Absolute Gene
22 Expression Profiles Reveals Distinct Regulation of Central Carbon Metabolism Genes in
23 Yeast'. Edited by Kevin J Verstrepen. *eLife* 10 (March): e65722.
24 <https://doi.org/10.7554/eLife.65722>.

25 Zavřel, Tomáš, Marjan Faizi, Cristina Loureiro, Gereon Poschmann, Kai Stühler, Maria Sinetova, Anna
26 Zorina, Ralf Steuer, and Jan Červený. 2019. 'Quantitative Insights into the Cyanobacterial Cell
27 Economy'. Edited by Severin Sasso, Ian T Baldwin, Severin Sasso, and Jörg Toepel. *eLife* 8
28 (February): e42508. <https://doi.org/10.7554/eLife.42508>.

29

1 **FIGURE LEGENDS**

2

3 **Figure 1: Characterisation of culture growth in turbidostats across eight minimal media.**

4 **A.** Illustration of the turbidostat culture chamber with the control flow and analysis pipeline. **B.**
5 Example growth curve (Ile replicate 2) showing different growth phases in the turbidostat. **C.**
6 Estimated growth rates μ based on a two-fold dilution and regrowth cycle for the 8 growth
7 media using 3 biological replicates each. Amm: ammonium chloride, equal to standard EMM2
8 medium. **D.** Total number of generations each culture spent in a turbidostat. **E.** Total time in
9 hours each culture spent in a turbidostat, with the duration of individual growth phases
10 coloured as in B. Note that, with N_G the number of generations, T the time spent in the
11 turbidostat, μ the growth rate, and T_d the doubling time, $T_d = \ln(2)/\mu$ and $N_G = T/T_d$.

12 **Figure 2: Fission yeast gene expression shows growth-rate dependent and nutrient-
13 specific components.** **A.** Hierarchical clustering of z-score transformed protein expression
14 fractions for the 2045 protein groups detected across all conditions for cells grown in 7 single
15 amino acids or NH₄Cl (Amm) using 3 biological replicates. Growth conditions are ordered by
16 increasing growth rate. Ten clusters are labelled on the left together with manual summary of
17 enriched functional categories (see Supp. Fig. S2.1). **B.** Summed protein mass fractions for
18 the 10 clusters defined in A as a function of the growth rate. Repeated-median linear model
19 (RMLM) fit is shown as a black line and the predicted 2.5th–97.5th percentile confidence interval
20 (CI) of the fit as the grey shaded area. **C.** As shown in B, for DESeq2-normalised RNA-Seq
21 counts. **D.** Assignment of 2077 proteins detected across all conditions and their respective
22 transcripts to the R (orange), P (blue), and Q (grey) sectors based on protein fractions (left)
23 and DESeq2-normalised counts (right). Each protein is connected to its corresponding
24 transcript by a line and colours are according to the protein sectors. **E.** Sum of protein fractions
25 for the R (orange), P (blue), and Q (grey) sectors as a function of growth conditions. The figure
26 includes all 3510 protein groups detected in at least one condition. Best fit and predicted CI
27 are plotted for the ordinary least squares (OLS) linear model. **F.** As shown in E, for DESeq2-
28 normalised RNA-Seq counts for 5135 detected genes. Abbreviations: P_P, Q_P, R_P: protein
29 groups assigned to P-, Q-, and R-sector. P_T, Q_T, R_T: transcripts corresponding to protein
30 groups detected across all conditions assigned to P-, Q-, and R-sector. P_T, Q_T, R_T: all
31 transcripts assigned to P-, Q-, and R-sector.

32 **Figure 3: Proteins from the R sector are involved in every level of the protein production
33 programme.** **A.** Fraction of R (orange), P (blue), and Q (grey) genes in manually curated
34 broad categories of protein complexes. The number of complexes (C) and genes (G) in each
35 category are shown in parentheses. The 4 leftmost categories encompass the protein
36 production programme. **B.** Volcano plot of protein complexes belonging to the broad
37 categories "snoRNA regulation", "Protein translation", "Ribosomal proteins", and "Ribosome
38 biogenesis" in the protein production programme. The plot shows the -log₁₀ of the q-value of
39 the repeated-median linear model (RMLM) fit on the sum of normalised counts in each protein
40 complex as a function of the growth rate against a normalised estimate of the slope of the fit
41 (see **Methods**). **C.** As shown in B for complexes belonging to the "mRNA regulation" and
42 "Chromatin regulation" categories. **D.** Sums of DESeq2-normalised counts for subunits of
43 RNAPI (left), II (middle) and III (right) are plotted as a function of the growth rate. The sums of
44 subunits unique to a given complex are plotted in orange and of all subunits are plotted in
45 grey. RMLM fits are shown as lines and the predicted 2.5th–97.5th percentile confidence
46 interval (CI) of the fit as shaded areas.

47 **Figure 4: Stoichiometries of translation complexes, comparison of ribosomal growth
48 law with other species, and functional analysis of P sector.** **A.** Sum of the protein fractions

1 plotted as a function of the growth rate for factors involved in translation initiation, elongation,
2 and termination (IET; left), ribosome biogenesis (RiBi; middle), or ribosomal proteins (RP;
3 right). The best fit and bootstrapped 95% confidence interval (CI) are shown in black and grey,
4 respectively. The fold change (FC) values \pm standard deviations of the bootstrapped values
5 are shown. **B.** Proteome mass ratio plotted as a function of the growth rate for the following
6 comparisons: IET vs RP (left), RiBi vs IET (middle), and RiBi vs RP (right). Shown in black/grey
7 are the predictions and 95% CIs as given by the linear models fitted to the data in A. **C.** FC
8 values for proteins of the IET, RiBi, and RP categories plotted as a function of their median
9 expression. Proteins assigned to the R, P, and Q sectors are coloured in orange, blue, and
10 grey, respectively. **D.** Total proteome mass fraction allocated to ribosomal proteins as a
11 function of growth rate for *S. cerevisiae* (red) (Metzl-Raz et al. 2017), *S. pombe* (green), and
12 *E. coli* (grey) (data from (A. Schmidt et al. 2016)). RMLM fits and 95% CIs are shown as lines
13 and shaded areas, respectively. **E.** The $-\log_{10}$ Q-value of repeated-median linear model
14 (RMLM) fits plotted against their respective FC values for proteins belonging to GO-slim and
15 literature lists (Mata et al. 2002; D. Chen et al. 2003; Rustici et al. 2004; Rallis, Codlin, and
16 Bähler 2013; Kamrad et al. 2020). List with a significant negative slope (q -value < 0.001) are
17 highlighted in blue. BP GO-slim terms related to metabolism are highlighted in green,
18 stress/growth modules from (D. Chen et al. 2003) in vermillion, and cell cycle induced modules
19 from (Rustici et al. 2004) in orange. **F.** Sum of protein fractions plotted as a function of the
20 growth rate for the Core Environmental Stress Response (CESR) repressed (growth module)
21 or induced (stress module) genes. RMLM fit and predicted 95% CI as in A. **G.** Assignment of
22 growth and stress module proteins (Prot) detected in all samples and their respective
23 transcripts (Trans) to the R (orange), P (blue), and Q (grey) sectors based on protein fraction
24 expression and DESeq2 normalised counts. Each protein is connected to its corresponding
25 transcript by a line and the colours correspond to the protein sectors.

26 **Figure 5: The coordination of energy metabolism enzymes with the growth rate is**
27 **marginal** **A.** Sum of protein fractions of proteins involved in translation and ribosome
28 biogenesis (red, see Figure 4A), energy metabolism and transport (green, see Figure 4E) or
29 all other genes (grey) plotted as a function of the growth rate. **B.** Relative proteome fractions
30 of 5 categories of proteins involved in metabolism. The median of the three replicates from
31 each condition was used for calculating the protein fractions and plotting growth rates. **C.** As
32 shown in B, for proteins of the OXPHOS and TCA pathways, the Adh1 and Pdc101
33 fermentation proteins, and proteins annotated as "generation of precursor metabolites and
34 energy" and not included in the other four categories or glycolysis. **D.** Protein expression as a
35 function of growth rate as exhibited by the first principal component (PC1). **E.** Comparison of
36 the first two principal components (PCA biplot) for each protein group detected in the proteome
37 across all conditions. Areas with $>50\%$ variance explained by PC1 correlation are highlighted
38 in yellow (negative correlation, WFSP-) and pink (positive correlation, WFSP+). Genes related
39 to glycolysis and ethanol fermentation are indicated in blue. **F.** Topology of the glycolysis and
40 ethanol fermentation pathway showing genes, cofactors, and selected metabolites, with
41 colours as in E. **G.** Left: ratio of protein fractions for Adh1/Tdh1 plotted as a function of the
42 growth rate. Right: diagram showing Adh1 and Tdh1 functioning together with median
43 proteome fractions of both proteins in each condition. Colours are as annotated in D. **H.** As
44 shown in G for Nde1 and Ndi1. **I.** Ratio of protein fractions of Idh2 and Idh1 plotted as a
45 function of the growth rate. Colours are as annotated in D. **J.** As shown in I for the ratio of the
46 protein fractions of Dld1 and Kgd1 plotted as a function of growth rate.

47 **Figure 6: Transcriptomic signatures for growth on amino acid sources.** **A.** DESeq2 \log_2
48 fold change ratios (scale capped at $\text{abs}(\log_2(fc)) = 5$) for the 10 signatures R1-R10. Fold
49 changes are relative to the RMLM-predicted synthetic reference (**Methods**). Columns are
50 ordered according to the growth rate and rows are ordered by hierarchical clustering (**Supp.**

1 **Fig. 6.1).** **B.** The \log_2 -transformed ratios of observed versus RMLM-predicted protein fractions
2 for genes in the R1-R10 signatures. Row and column orders are as described in A. Genes
3 missing from the proteomics data are in grey. **C.** Functional analysis of the transcriptomics
4 clusters R1-R10 as shown in A. Enrichment for GO slim terms belonging to the “biological
5 process” (top), “cellular component” (middle), and “molecular function” (bottom) categories are
6 shown. The colour scheme denotes the local false discovery rate (lfd , capped at $1e^{-6}$ and
7 printed on the figure if capped) from a Fisher exact one-sided test for the overlap of each
8 cluster with functional lists. Only significant lists are shown ($lfd < 0.05$) and the number of
9 genes in each category and cluster are shown in parentheses.

10

1 **SUPPLEMENTARY FIGURE LEGENDS**

2

3 **Supplementary Figure S2.1: Functional analysis of the proteome clusters from Figure**
4 **2A.** Enrichment for GO slim terms belonging to the “biological process” (top), “cellular
5 component” (middle), and “molecular function” (bottom) categories are shown. The colour
6 scheme denotes the local false discovery rate ($lfdr$, capped at $1e^{-6}$ and printed on the figure if
7 capped) of a Fisher exact one-sided test for the overlap of each cluster with the functional
8 lists. Only significant lists are shown ($lfdr < 0.05$) and the number of genes in each category
9 and cluster are shown in parentheses.

10 **Supplementary Figure S2.2: mRNA dependence on the growth rate.** Hierarchical
11 clustering of the z-score transformed DESeq-normalised RNA-Seq counts for 4979 mRNAs
12 expressed across all conditions in the RNA-Seq dataset for cells grown on 7 single amino
13 acids or NH₄Cl (Amm). The growth conditions are ordered by increasing growth rate. The
14 twelve clusters are indicated on the left. **B.** Sum of DESeq-normalised RNA-Seq counts for
15 the 12 clusters defined in A as a function of growth conditions. The growth conditions are
16 ordered by increasing growth rate. The RMLM best fit is shown in black and the predicted 95%
17 confidence interval in grey.

18 **Supplementary Figure S2.3: ncRNA dependence on the growth rate I.** Hierarchical
19 clustering of z-score transformed DESeq-normalised RNA-Seq counts for 1211 ncRNAs for
20 cells grown on 7 single amino acids or NH₄Cl (Amm). The growth conditions are ordered by
21 increasing growth rate. The nine clusters are labelled on the left. **B.** Sum of DESeq2-
22 normalised RNA-Seq counts for the 9 clusters defined in A as a function of growth conditions.
23 The growth conditions are ordered by increasing growth rate. The RMLM best fit is shown in
24 black and the predicted 95% confidence interval in grey. **C.** The z-score transformed DESeq2-
25 normalised RNA-Seq counts of all genes that neighbour the ncRNAs from the clusters defined
26 in A are shown. Annotations of flanking genes were taken from (Atkinson et al. 2018). **D.** Sum
27 of DESeq2-normalised RNA-Seq counts (NC) for the neighbouring genes for each cluster
28 defined in A.

29 **Supplementary Figure S2.4: Illustration of repeated-median linear model (RMLM) fits on**
30 **single genes.** **A.** Example R-protein Rpl402. **B.** Example P protein Suc22. **C.** Example Q
31 protein group comprising Hht1, Hht2, and Hht3. **D.** Example of P protein with additional
32 medium-specific expression Snz1. **E.** Example WFSP+ pattern (see Fig. 5D) with a poor
33 RMLM fit for the protein group comprising Ubi3, Ubi4, and Ubi5. **F.** Additional example of a
34 poor RMLM fit for the protein Mae2. The best fit for the RMLM is shown as solid black lines
35 and the predicted 95% CI in grey. The best fit for the ordinary least squares (OLS) linear model
36 is shown as dashed grey lines. **G.** Illustration of the fold change (FC) calculation for the
37 example protein Rpl402 indicating the relationship between the FC values, slope, and the y-
38 intercept of the fit. **H.** Growth law shapes corresponding to a series of example FC values.

39 **Supplementary Figure S2.5: Growth category assignment of proteins and the**
40 **corresponding transcripts from clusters defined in Figure 2A.** Assignment of proteins
41 from the clusters defined in Figure 2A (Prot) and their respective transcripts (Trans) in the R
42 (orange), P (blue), and Q (grey) sectors based on protein fraction expression and DESeq2-
43 normalised counts. Each protein is connected to its corresponding transcript by a line coloured
44 as per the protein classification.

45 **Supplementary Figure S3.1 Volcano plot of protein complexes that do not belong to**
46 **those illustrated in Figure 3B-C.** The $-\log_{10}$ of the q -value of the repeated-median linear

1 model (RMLM) fit on the sum of normalised counts in each protein complex as a function of
2 the growth rate are plotted against a normalised estimate of the slope of the fit (see **Methods**).

3 **Supplementary Figure S4.1: Stoichiometries of translation complexes as a function of**
4 **the growth rate.** **A.** Bootstrapped parameter densities of fold change (FC), slope and intercept
5 values for the IET (blue), RiBi (pink), and RP (red) categories. The analysis is based on the
6 1000 bootstrap samples used in Figures 4A and B. **B.** The sum of protein fractions in the
7 translation “Initiation”, “Elongation”, and “Termination” categories plotted as a function of the
8 growth rate. The best fit and bootstrapped 95% CI are shown in black and grey, respectively.
9 The FC values \pm standard deviations of bootstrapped values are shown. **C.** The proteome
10 mass ratio plotted as a function of the growth rate for the following comparisons: Elongation
11 vs Initiation (left), Termination vs Initiation (middle), and Termination vs Elongation (right).
12 Shown in black and grey are the predictions and 95% CIs, respectively, as given by the linear
13 models fitted to the data in B.

14 **Supplementary Figure S4.2: Analysis of translational proteins with non-positive or**
15 **weak growth-rate correlations.** **A.** Normalised sum of squared residuals (SSR) versus
16 coefficient of determination (R^2) for repeated-median linear model (RMLM) fits to protein
17 groups involved in translation initiation, elongation, and termination (IET, left), ribosome
18 biogenesis (RiBi, middle), and to ribosomal proteins (RP, right). All P-sector proteins were
19 labelled, R-sector proteins were labelled if their normalised SSR was greater than 0.1; for Q-
20 sector proteins the threshold was 0.2. **B.** Proteome burden associated with translation
21 elongation and termination factor eIF5A (Tif512) as a function of growth rate. The best fitted
22 RMLM is shown as a solid black line, with its predicted 95% CI in grey. The best fitted ordinary
23 least squares model is shown as a dashed grey line. **C.** As shown in B for translation initiation
24 factor eIF3e (Int6). **D.** Ratio of protein mass fractions for Int6 and the major eIF3 subunit Tif301
25 plotted as a function of the growth rate.

26 **Supplementary Figure S4.3: Stoichiometries of translation complexes as a function of**
27 **the growth rate in *E. coli*** (A. Schmidt et al. 2016). **A.** Sum of the protein fractions plotted as
28 a function of the growth rate for factors involved in translation initiation, elongation, and
29 termination (IET, left), ribosome biogenesis (RiBi, middle), or for ribosomal proteins (RP, right).
30 The best fit and bootstrapped 95% confidence interval (CI) are shown in black and grey,
31 respectively. The fold change (FC) values \pm standard deviations of the bootstrapped values
32 are shown. The type of nutrient or perturbation used to modulate the growth rate are colour
33 coded as per the legend on the right. Data from cultures in stationary phase was not included
34 in the fits. **B.** The proteome mass ratio plotted as a function of the growth rate for the following
35 comparisons: IET vs RP (left), RiBi vs IET (middle), and RiBi vs RP (right). Shown in black
36 and grey are the predictions and 95% CIs, respectively, as given by the linear models fitted to
37 the data in A. **C.** FC values for proteins of the IET, RiBi, and RP categories plotted as a function
38 of their median expression. Proteins assigned to the R, P, and Q sectors are coloured in
39 orange, blue, and grey, respectively.

40 **Supplementary Figure S4.4: Analysis of the residuals of the R and P sectors.** **A.** Violin
41 plots and box plots of the normalised sum of squared residuals (SSR) of the RMLM best fit for
42 mRNA counts or protein fractions belonging to the R (orange) or P (blue) sectors. The *p*-values
43 for the two-sided Wilcoxon rank-sum test are indicated. **B.** As shown in A for the R^2 values. **C.**
44 Normalised SSR of the RMLM fit plotted against their respective R^2 values for all proteins
45 belonging to the R (orange), P (blue), or Q (grey) sectors. **D.** As shown in C for clusters 1 (left),
46 4 (middle) and 8 (right) of Figure 2A.

47 **Supplementary Figure S4.5: Functional analysis of P sector mRNAs.** **A.** The $-\log_{10} q$ -
48 value of RMLM fits plotted against their respective FC values for mRNAs belonging to the GO-

1 slim and literature lists (Mata et al. 2002; D. Chen et al. 2003; Rustici et al. 2004; Rallis, Codlin,
2 and Bähler 2013; Kamrad et al. 2020). The lists with a significant negative slope (q -value <
3 0.001) are highlighted in blue. The BP GO-slim terms related to metabolism are highlighted in
4 green, stress/growth modules from (D. Chen et al. 2003) in vermillion, and cell cycle induced
5 modules from (Rustici et al. 2004) in orange. **B.** Sum of the DESeq2-normalised counts plotted
6 as a function of the growth rate for the Core Environmental Stress Response (CESR)
7 repressed (growth module), or the induced (stress module) genes. The RMLM fit and predicted
8 95% CI are indicated as in Figure 4F. **C.** The sum of protein fractions plotted as a function of
9 the growth rate for S phase induced periodic genes (Rustici et al. 2004). **D.** As shown in C for
10 the DESeq2 normalised counts. **E.** Total expression in RNA-Seq (DESeq2-normalised counts,
11 left panel) and proteomics data sets (proteome fraction, right panel) for gene lists induced in
12 the M phase versus G1 phase (Rustici et al. 2004).

13 **Supplementary Figure S4.6: Functional enrichment of P sector proteins.** The $-\log_{10}$ of q -
14 value (tail-based false discovery rate) of the one-sided Fisher exact enrichment test plotted as
15 a function of the number of genes detected across all conditions in the proteome for all *S.*
16 *pombe* GO-slim categories. Significantly enriched lists (q -value < 0.05) are highlighted in cyan.
17 The BP GO-slim terms related to metabolism are highlighted in green.

18 **Supplementary Figure S5.1: Growth rate specificity of metabolism proteins (related to**
19 **Figure 5B).** Sum of protein fractions plotted as a function of the growth rate for 6 categories
20 covering metabolism (see Figure 5B and Methods).

21 **Supplementary Figure S5.2: Growth rate specificity of energy metabolism proteins**
22 **(related to Figure 5C).** Top left two panels: protein fractions as a function of growth rate for
23 the ethanol fermentation enzymes Adh1 and Pdc101. Remaining three panels: sum of protein
24 fractions as a function of growth rate for the proteins involved in oxidative phosphorylation,
25 TCA cycle, and for those annotated as "generation of precursor metabolites and energy" and
26 that were neither included in the first four panels nor glycolysis.

27 **Supplementary Figure S5.3: Condition specific expression of complexes forming the**
28 **respiratory electron transport chain and proton pumps.** The sum of protein mass fractions
29 as a function of the growth rate (top panels) and median proteome fraction of components of
30 the complex in each condition (bottom panels), for internal NADH dehydrogenase, the
31 succinate dehydrogenase complex, the cytochrome C reductase complex, cytochrome C, the
32 cytochrome C oxidase complex, and the ATP synthases.

33 **Supplementary Figure S5.4: PCA analysis of the proteomics data.** **A.** Cumulative variance
34 explained by the first 9 principal components of the proteomics dataset (**Methods**). **B.** PC1
35 plotted against PC2 for all proteins belonging to the R (orange), P (blue), or Q (grey) sectors.
36 **C.** As shown in B for PC3 and PC1. **D.** As shown in B for PC3 and PC2. **E.** The relative
37 contribution of each experimental condition plotted as a function of the growth rate for the first
38 9 principal components of the proteomics dataset. Note that PC1 shows a clear WFSP+
39 pattern, as repeated in Figure 5D.

40 **Supplementary Figure S5.5: Proteome burdens of enzymes in the glycolysis and**
41 **ethanol fermentation pathways.** Repeated-median linear model fits are shown as black lines
42 and the predicted 2.5th–97.5th percentile confidence intervals of the fits as the grey shaded
43 areas.

44 **Supplementary Figure S5.6: Proteome burdens of selected enzymes with NAD cofactor**
45 **(related to Figure 5I–J).** Repeated-median linear model fits are shown as black lines and the
46 predicted 2.5th–97.5th percentile confidence intervals of the fits as the grey shaded areas.

1 **Supplementary Figure S6.1: Hierarchical clustering of RNA-Seq data after correction**
2 **for growth-rate dependent gene expression.** Counts were normalised to the growth-
3 dependent linear model in DESeq2 and the fold change ratios fc were calculated with respect
4 to a synthetic average sample as a reference (**Methods**). Only genes with at least one
5 condition meeting $\text{abs}(\log_2(fc)) > 0.5$ and adjusted p -values < 0.01 were selected. Gene-
6 condition pairs not meeting this significance threshold are shown in grey. The colour scale is
7 capped at $\text{abs}(\log_2(fc)) = 5$. The R1-R10 signatures from Figure 6 are shown on the left.

8 **Supplementary Figure S6.2: Functional analysis focusing on informative terms of R1-**
9 **R10 signatures from Figure 6.** Enrichment for GO terms belonging to the “biological process”
10 category with no more than 50 annotations are shown. The colour scheme denotes the $-\log_{10}$
11 local fdr ($lfdr$, capped at $1e^{-9}$) for Fisher exact one-sided tests for the overlap of each cluster
12 with functional lists. Only significant lists are shown ($lfdr < 0.01$) and the number of genes in
13 each category and clusters are shown in parentheses.

14

1 **SUPPLEMENTARY TABLE LEGENDS**

2

3 **Supplementary Table S1: Summary of growth conditions for the 24 cultures studied.**

4 medium: three-letter abbreviation of growth medium; replicate: biological replicate index;
5 growth_rate: calculated growth rate (in h⁻¹); doubling_time: doubling time as calculated from
6 the growth rate (in h); OD: mean OD₆₀₀ during second phase of stable OD; total_doublings:
7 total number of doubling times elapsed during turbidostat growth; growth_1_h: elapsed time
8 (in h) between inoculation and first meeting of the OD setpoint; constant_2_h: elapsed time
9 (in h) during the initial phase of stable growth; dilution_h: elapsed time (in h) during the
10 approximate twofold dilution; growth_2_h: elapsed time (in h) during regrowth phase following
11 the dilution; constant_2_h: elapsed time (in h) during the second phase of stable OD; total_h:
12 total elapsed time (in h) during turbidostat growth; nitrogen_source: full name of nitrogen
13 source in growth medium; turbidostat: index of physical device that the culture was grown in.

14 **Supplementary Table S2: Summary of protein groups detected in proteomics analysis.**

15 PomBaseIDs: database identifiers of the proteins comprising the protein group, i.e that were
16 indistinguishable based on the detected peptides; n_proteins: number of proteins comprising
17 the group; Protein IDs: FASTA headers of the proteins; total_peptides_all: number of different
18 peptides detected in at least one sample that could have been assigned to the group;
19 total_peptides_razor: number of different peptides detected in at least one sample that were
20 assigned to the group; total_peptides_unique: number of different peptides detected in at least
21 one sample that were assigned to the group and could not have been assigned to another
22 group; sequence_coverage: percentage of the protein sequence that overlapped with at least
23 one peptide; sequence_lengths: number of amino acids comprising the group's proteins'
24 peptide chain; mol_weight: molecular weight of protein (in kDa).

25 **Supplementary Table S3: Relative protein expression levels as determined by the**
26 **proteomics analysis.** PomBaseIDs: database identifiers of the protein group; medium: three-
27 letter abbreviation of growth medium; replicate: biological replicate index; iBAQ: intensity
28 based absolute quantification; raw: raw detected intensity; lfq: label-free quantification as
29 reported by MaxQuant.

30 **Supplementary Table S4: Proteome mass fractions as determined from intensity-based**
31 **absolute quantifications (iBAQ).** PomBaseIDs: database identifiers of the protein group;
32 medium: three-letter abbreviation of growth medium; replicate: biological replicate index;
33 proteome_fraction: proteome mass fraction.

34 **Supplementary Table S5: Transcript abundance as determined by RNA-Seq analysis**
35 **and subsequent normalisation.** PomBaseIDs: database identifiers of the protein group;
36 medium: three-letter abbreviation of growth medium; replicate: biological replicate index;
37 normalised_counts: abundance after DESeq2-based normalisation; rpkm: reads per kilobase
38 per million; raw_counts: raw counts detected in sequencing analysis.

39 **Supplementary Table S6: Summary statistics of repeated-median linear model (RMLM)**
40 **fits and of gene expression.** PomBaseID: systematic database identifier of the gene;
41 primary_name: gene standard name; description: gene product description; PomBaseIDs:
42 proteomics protein group identifier; sector.proteins: proteome sector the protein group was
43 assigned to (*q*-value < 0.1); confident.proteins: whether proteome assignment was confident
44 (local false discovery rate *lfdr* < 0.1); cluster.proteins: cluster the protein group was assigned
45 to (see Fig. 2A); sector.transcripts: transcriptome sector the protein group was assigned to (*q*-
46 value < 0.1); confident.transcripts: whether transcriptome assignment was confident (*lfdr* <

1 0.1); cluster.transcripts: cluster the transcript was assigned to (see Supp. Fig. 2.2A);
2 q.value.proteins: *q*-value assigned to the protein RMLM fit; local_fdr.proteins: *lfdr* assigned to
3 the protein RMLM fit; slope.proteins: slope of the protein RMLM fit; intercept.proteins: *y*-
4 intercept of the protein RMLM fit; p.value.proteins: *p*-value associated with the protein RMLM
5 fit; r.squared.proteins: coefficient of determination (R^2) of the protein RMLM fit; fc.proteins: fold
6 change (FC) calculated from the protein RMLM fit; median.proteins: median proteome mass
7 fraction; max.proteins: largest detected proteome mass fraction; min.proteins: smallest
8 detected proteome mass fraction; spread.proteins: difference between largest and smallest
9 detected proteome mass fraction; n_conditions.proteins: number of conditions that the protein
10 was detected in; mean.proteins: mean proteome mass fraction; var.proteins: variance of
11 proteome mass fraction; cv.proteins: coefficient of variation (CV) of proteome mass fraction;
12 ssr.proteins: sum of squared residuals (SSR) to the RMLM for proteome mass fractions;
13 norm_ssrr.proteins: normalised SSR for proteome mass fractions (see **Methods**, equation (7)
14); q.value.transcripts: *q*-value assigned to the transcript RMLM fit; local_fdr.transcripts: *lfdr*
15 assigned to the transcript RMLM fit; slope.transcripts: slope of the transcript RMLM fit;
16 intercept.transcripts: *y*-intercept of the transcript RMLM fit; p.value.transcripts: *p*-value
17 associated with the transcript RMLM fit; r.squared.transcripts: R^2 of the transcript RMLM fit;
18 fc.transcripts: FC calculated from the transcript RMLM fit; median.transcripts: median RNA-
19 Seq normalised counts; max.transcripts: largest detected RNA-Seq normalised counts;
20 min.transcripts: smallest detected RNA-Seq normalised counts; spread.transcripts: difference
21 between largest and smallest detected RNA-Seq normalised counts; n_conditions.transcripts:
22 number of conditions that the transcript was detected in; mean.transcripts: mean RNA-Seq
23 normalised counts; var.transcripts: variance of RNA-Seq normalised counts; cv.transcripts:
24 CV of RNA-Seq normalised counts; ssr.transcripts: SSR to the RMLM for RNA-Seq
25 normalised counts; norm_ssrr.transcripts: normalised SSR for RNA-Seq normalised counts
26 (see **Methods**, equation (7)).

27 **Supplementary Table S7: Manual assignment of complexes to broader functional**
28 **categories.** GOID: Gene Ontology (GO) term accession identifier; description: GO term
29 name; category: manually assigned category.

30 **Supplementary Table S8: Assignment of *S. pombe* translation proteins to non-**
31 **overlapping functional classes.** PomBaseIDs: proteomics protein group identifier;
32 annotation: annotation to ribosomal protein (RP), initiation/elongation/termination factors
33 (IET), or ribosome biogenesis (RiBi).

34 **Supplementary Table S9: Assignment of *E. coli* translation genes to non-overlapping**
35 **functional classes.** gene: gene identifier; annotation: annotation to ribosomal protein (RP),
36 initiation/elongation/termination factors (IET), or ribosome biogenesis (RiBi).

37 **Supplementary Table S10: Assignment of metabolic proteins to non-overlapping**
38 **functional classes.** PomBaseIDs: proteomics protein group identifier; annotations: all
39 relevant GO-slim annotations present for the protein group (semi-colon-separated); class:
40 assignment to broad non-overlapping groups (**Fig. 5B**, **Supp. Fig. S5.1**); subclass: for
41 Precursors/Energy class, subdivision into non-overlapping subgroups (**Fig. 5C**, **Supp. Fig.**
42 **S5.2**).

43 **Supplementary Table S11: Proteins induced and repressed in Trp (W), Phe (F), Ser (S),**
44 **and Pro (P) media.** PomBaseIDs: proteomics protein group identifier; correlation: Pearson
45 correlation coefficient R between z-score transformed proteome mass fractions and protein
46 principal component 1 (PC1); r.squared: R^2 , WFSP: whether $R>0$ (+) or $R<0$ (-); PomBaseID:

1 systematic database identifier of the gene; primary_name: gene standard name; description:
2 gene product description.

3 **Supplementary Table S12: Differential expression analysis after removal of growth rate**
4 **correlations and subsequent assignment to transcriptional signatures.** PomBaseID:
5 gene identifier; cluster: assignment to transcriptional signature; medium: ; baseMean: baseline
6 transformed expression in synthetic reference; log2fc: log₂-transformed fold change; stderror:
7 standard error of the log₂-transformed fold change; statistic: test statistic of the DE analysis;
8 p.value: raw *p*-value of Wald test; p.adjusted: Benjamini–Hochberg adjusted *p*-value.

9

1

2 MATERIALS AND METHODS

3 Culture conditions

4 Cells were grown in continuous culture in turbidostats using Edinburgh minimal media (EMM2)
5 with saturating amounts of carbon and nitrogen (Petersen and Russell 2016). This ensured
6 that the cells could reach balanced exponential growth, limited only by internal gene
7 expression patterns. In addition to the standard EMM2 media where nitrogen is provided by
8 93.5 mM of ammonium chloride (NH₄Cl, referred to as Amm), we used seven alternative
9 nitrogen sources where 20 mM of a single amino acid replaced the NH₄Cl: glutamate (Glu),
10 proline (Pro), isoleucine (Ile), serine (Ser), phenylalanine (Phe), glycine (Gly), and tryptophan
11 (Trp) (Sigma).

12 Cells were grown and harvested as follows: 972h⁻ cells from frozen glycerol stocks were
13 precultured on YES agar plates. Single colonies were inoculated in 5-10 ml of EMM2 in glass
14 flasks and grown overnight at 32 °C. Approximately 1 ml of culture was transferred to a fresh
15 flask containing EMM2 and the final nitrogen source and grown to large ~5 x 10⁶ cells/ml.
16 These cells were used to inoculate the continuous culture setup at 0.5-1 x 10⁶ cells/ml. The
17 process was repeated for biological triplicates grown from three different colonies.

18 To generate the final cultures, cells were grown in turbidostats (Takahashi et al. 2015), with
19 media flow controlled using customised Python scripts (Saint et al. 2019). Cell cultures were
20 monitored every 30 s and fresh growth medium was added whenever the optical density OD₆₀₀
21 exceeded 0.4. This resulted in 1%–2% dilution cycles, keeping the total culture volume
22 constant throughout. Cells were kept in the turbidostats for ~10 generations at 32 °C. To
23 measure the growth rate, cells were diluted twofold approximately halfway through the
24 experiment and regrown to the reference level of OD₆₀₀ = 0.4. The growth rate for each sample
25 was determined by fitting an exponential curve to the OD measures acquired every 30 s during
26 the regrowth phase. The final culture volumes were ~30 ml, from which 10 ml was used for
27 transcriptomics, 10 ml for proteomics analysis, and 10 ml was saved as a backup. The cells
28 were harvested by centrifugation, washed twice with PBS and stored at -80 °C until RNA-Seq
29 and proteomics sample preparation was performed.

30 RNA-Seq

31 A 10 ml aliquot of the culture was centrifuged at 3000 rpm for 3 min. After removing the
32 supernatant, cell pellets were frozen in dry ice and kept at -80 °C until the library preparation
33 was performed. Total RNA from the pellets was extracted using the hot-phenol method (Lyne
34 et al. 2003) and the RNA obtained was quantified using a BioDrop (biochrom, Cambridge,

1 UK). Poly(A) enrichment was performed using 500 ng of total RNA with the NEBNext Poly(A)
2 mRNA Magnetic Isolation Module (NEB, Ipswich, USA) kit according to the manufacturer's
3 instructions. The remaining mRNA was used for stranded RNA-seq library preparation using
4 the NEBNext® Ultra™ II Directional RNA Library Prep Kit for Illumina® (NEB, Ipswich, USA)
5 according to the manufacturer's instructions. The resulting libraries were quality checked and
6 quantified using the Bioanalyser (Agilent, Santa Clara, USA) and a Qubit™ dsDNA BR Assay
7 Kit (Invitrogen) respectively.

8 Libraries were sequenced on an Illumina HiSeq 2500 instrument (Illumina, San Diego, USA).
9 Data were processed using RTA version 1.18.54 and 1.18.64, with default filter and quality
10 settings. The reads were demultiplexed with CASAVA 1.8.4 and 2.17 (allowing 0
11 mismatches). Transcripts were mapped to the genome sequences (available from PomBase)
12 using TopHat2 (Kim et al. 2013; Lock et al. 2019). HTSeq was used to count the number of
13 reads per exon (gff3, PomBase) (Anders, Pyl, and Huber 2015; Lock et al. 2019). The reads
14 across exons were summed to obtain the total number of reads per gene. This procedure
15 yielded raw counts c_{ijk} for each gene i , growth medium j , and biological replicate k . Per sample
16 normalisation was performed using the DESeq2 *estimateSizeFactors* function, yielding size
17 factors S_{jk} for each sample (Love, Huber, and Anders 2014). The normalised counts were
18 calculated as follows:

$$19 \quad n_{ijk} = \frac{c_{ijk}}{S_{jk}}. \quad (1)$$

20 Unless otherwise noted, RNA-Seq analyses were performed using these normalised counts,
21 which enabled between-sample comparison of the expression of genes or sets of genes.

22 Proteomics

23 Cell pellets from 10 ml of each turbidostat culture was frozen in dry ice and stored at -80 °C
24 until sample preparation. Once thawed, cells were resuspended in lysis buffer (1% sodium
25 deoxycholate, 1% ammonium bicarbonate). Lysis was performed in a FastPrep instrument
26 (MP Biomedical) for 5 pulses at a speed of 6 m/s. Total cell extracts were treated with 5 mM
27 tris(2-carboxyethyl)phosphine (TCEP) for 15 min at room temperature to reduce the disulphide
28 bonds. An alkylation reaction was performed with the addition of 10 mM iodoacetamide for 30
29 min at 25 °C in the dark. The reaction was quenched using 12 mM N-acetyl-cysteine for 10
30 min. The proteins were quantified using a BCA Protein Assay Reducing Agent Compatible kit
31 (ThermoFisher Scientific) and 100 µg of total protein was used for digestion. To improve the
32 cleavage efficiency, protein extracts underwent a double digestion, first with Lys-C (Wako
33 chemicals, USA) for 4 h at 37 °C using a 1:200 (w/w) ratio, and then overnight with porcine
34 trypsin at 37 °C using a 1:100 (w/w) ratio. Digestion was stopped by lowering the pH with

1 trifluoroacetic acid (TFA) at a final volume of 1%. The sodium deoxycholate precipitate formed
2 due to the lowered pH was removed by centrifuging the samples at 4 °C for 15 min at 14,000
3 rpm. The precipitated detergent was then discarded. The digested peptides were vacuum
4 dried and stored at -80 °C until required for analysis.

5 The protein digests were analysed by liquid chromatography-tandem mass spectrometry (LC-
6 MS/MS) via an untargeted analysis approach using Data-Dependent Acquisition (DDA)
7 (Ducret et al. 1998). The raw MS data was analysed using MaxQuant (Cox and Mann 2008)
8 and applying the Label-free Quantification algorithm (Cox et al. 2014) for DDA data analysis.

9 Protein digests were reconstituted in 0.1% trifluoroacetic acid (TFA) and transferred to
10 autosampler vials for LC-MS/MS analysis. The tryptic peptides were separated using an
11 Ultimate 3000 RSLC nano liquid chromatography system (Thermo Scientific) coupled to a Q-
12 Exactive tandem mass spectrometer (Thermo Scientific) via an EASY-Spray source. Sample
13 volumes were loaded onto a trap column (Acclaim PepMap 100 C18, 100 μ m x 2 cm) at 8
14 μ l/min of 2% acetonitrile, 0.1% TFA. Peptides were eluted on-line to an analytical column
15 (EASY-Spray PepMap C18, 75 μ m x 75 cm). Peptides were separated at 200 nl/min with a
16 ramped 180 min gradient using 4%-30% buffer B (buffer A: 2% acetonitrile, 0.1% formic acid;
17 buffer B: 80% acetonitrile, 0.1% formic acid) over 150 min, and 30%-45% buffer B over 30
18 min. Eluted peptides were analysed by operating in positive polarity using a data-dependent
19 acquisition mode. Ions for fragmentation were determined from an initial MS1 survey scan at
20 70,000 resolution (at m/z 200) in the Orbitrap followed by Higher-energy Collisional
21 Dissociation (HCD) of the top 12 most abundant. MS1 and MS2 scan AGC targets set to 3e6
22 and 5e4 for maximum injection times of 50 ms and 110 ms, respectively. A survey scan
23 covering the range of 400–1800 m/z was used, with HCD parameters of isolation width 2.0
24 m/z and a normalised collision energy of 27%.

25 DDA data was processed using the MaxQuant software platform (v1.6.2.3) (Cox and Mann
26 2008) with database searches performed by the in-built Andromeda search engine against the
27 PomBase database (5,138 entries, v.20190507) (Lock et al. 2019). A reverse decoy database
28 was created, and the results displayed at a 1% false discovery rate (fdr) for peptide spectrum
29 matches and identified proteins. The search parameters included trypsin, two missed
30 cleavages, fixed modification of cysteine carbamidomethylation, and variable modifications of
31 methionine oxidation, asparagine deamidation, N-terminal glutamine to pyroglutamate
32 modification, and protein N-terminal acetylation. Label-free quantification was enabled with an
33 LFQ minimum ratio count of 2. The ‘match between runs’ function was used with match and
34 alignment time limits of 0.7 and 20 min, respectively.

1 Intensities were based on identified unique and razor peptides, and intensity-based absolute
2 quantification (iBAQ) was calculated as the raw intensity/number of obtainable tryptic
3 peptides. For the post-processing of the MaxQuant output, the data was filtered for detection
4 in all three biological replicates. Subsequently, proteome mass fractions ϕ_{ij} were calculated for
5 each protein group i , sample from growth medium j , replicate k from the reported protein
6 masses m_i , and the iBAQ quantities B_{ijk} as follows:

7

$$\phi_{ijk} = \frac{m_i B_{ijk}}{\sum_l m_l B_{ljk}}. \quad (2)$$

8 **Repeated median linear models**

9 As shown in the main text, several genes were enriched in one or more growth conditions in
10 addition to growth-rate correlations. The presence of such outliers affected the fit quality of the
11 standard ordinary least squares (OLS) linear model fits. To account for this, we used repeated
12 median linear models (RMLM) for fitting regression lines (Siegel 1982), as implemented in the
13 R package `mblm` (Komsta 2019). This method is robust when up to 50% of outliers are
14 present in the data, and the working is described below.

15 In general, the data can be described as N pairs of the growth rate μ and some expression
16 value y ($N = 24$ if expression was detected across all samples, or a smaller multiple of 3 when
17 data was missing). From each observation $(\mu, y)_i$, a line is drawn to each of the other $N - 1$
18 points $(\mu, y)_j$, and the median slope and y -intercept of these $N - 1$ lines is associated with the
19 data point i . The regression coefficients for the slope and y -intercept of the repeated median
20 linear model are defined as the medians of all N slopes and y -intercepts. To compare the
21 growth law shape of protein groups with varying absolute abundances, the fold-change FC
22 was defined from the RMLM as the ratio

23

$$FC = \frac{y(\mu = \mu_{\max}) - y(\mu = 0)}{y(\mu = 0.5\mu_{\max})}, \quad (3)$$

24

25 with $\mu_{\max} = 0.3 \text{ h}^{-1}$. This can be expressed in terms of the fitted slope a and the y -intercept b
26 as follows:

27

$$FC = \frac{\mu_{\max}}{0.5\mu_{\max} + b/a}. \quad (4)$$

28 **Hierarchical clustering**

29 We used z-scores to normalise for variations in absolute expression levels. For each gene or
30 protein group i in the sample with medium j and replicate k , the z-score was calculated as

1

$$z_{ijk} = \frac{y_{ijk} - \mu_i}{\sigma_i} \quad (5)$$

2 from the expression values y_{ijk} , where μ_i and σ_i are the mean and standard deviations across
3 all samples. The analysis was performed only on genes or protein groups that were detected
4 across all 24 samples. The resulting matrices of the z-scores were analysed using hierarchical
5 clustering and principal component analysis.

6 Hierarchical clustering on genes/protein groups was performed using the Euclidean distance
7 and Ward linkage ("ward.D2"), using the `hclust` implementation of the R statistical language
8 (v.3.5.3). In the transcriptome analysis, separate dendograms were constructed for coding
9 and non-coding RNAs, using the protein-coding list from PomBase and selecting ncRNAs from
10 the presence of "NCRNA." in the systematic IDs.

11 **Sector assignment**

12 For each gene or protein group i , we calculated R-squared (R^2), defined as

13

$$R_i^2 = 1 - \frac{\sum_{j,k} r_{ijk}^2}{\sum_{j,k} (y_{ijk} - \mu_i)^2}, \quad (6)$$

14 and the associated p -values using the `summary.lm` method. Here r_{ijk} denotes the residuals
15 from the RMLM fit, y_{ijk} the expression (normalised counts or proteome fractions), μ_i the mean
16 expression across samples, and the summation was performed across all N samples where
17 the gene was detected. We calculated the tail-based false discovery rates (fdr , or q -values)
18 and local false discovery rates (fdr) using the `fdrtool` R package and the false non-discovery
19 rate cut-off method (Strimmer, 2008). Genes or protein groups were assigned to the P or R
20 sector when their tail-based $fdr < 0.1$. R and P sector genes had positive and negative slopes,
21 respectively, as determined by the fitted RMLM. In **Supp. Table S6**, hits with local $fdr < 0.1$
22 were flagged as confident.

23 To assess fit quality, in addition to R^2 , we used a normalised sum of squared residuals, defined
24 as

25

$$SSR_{\text{norm},i} = \frac{1}{N-1} \frac{\sqrt{\sum_{j,k} r_{ijk}^2}}{\mu_i}, \quad (7)$$

26 with the notations as described in the previous paragraph.

27 **Bootstrapping**

28 For the analysis illustrated in **Fig. 4AB** and **Supp. Fig. S4.1 and S4.3**, 1000 bootstrap samples
29 were generated using the `bootstraps` function from the `rsample` package (v0.0.8) (Silge et al.

1 2021). The RMLM analysis was repeated on the bootstrapped samples, resulting in sample
2 distributions for the RMLM slopes, intercepts, and FCs. Plots of the 2.5%-97.5% confidence
3 interval were drawn using the RMLM predictions on a 101-point grid spanning 0 to 0.3 h⁻¹.

4 Other confidence intervals were drawn using the *geom_smooth* function in ggplot2 (v3.3.2)
5 (Wickham 2016) with the default 95% confidence interval and the RMLM method, unless
6 otherwise noted.

7 **Barcode plots**

8 For the barcode plots in **Supp Fig. S4.3 and S4.6**, the directed length l_{ij} of the bar for protein
9 i and medium j was calculated from the median proteome mass fractions across the three
10 biological replicates,

11
$$x_{ij} = \text{median}_{k=1,2,3} \phi_{ijk}, \quad (8)$$

12 and the median across all samples,

13
$$M_i = \text{median}_{j,k} \phi_{ijk}, \quad (9)$$

14 in the following way:

15
$$l_{ij} = \frac{x_{ij} - M_i}{M_i}, \quad (10)$$

16 with missing data imputed to zero. The scale was capped at $-1 < l_{ij} < 2$.

17 **Differential expression analysis**

18 To identify differential expression in the transcriptome on top of growth rate mediated effects,
19 we performed an analysis using 'DESeq2' (v1.22.2) from the Bioconductor suite (v3.8) (Love,
20 Huber, and Anders 2014; Huber et al. 2015), comparing the residual expression in each
21 condition to a synthetic reference condition. The fold change obtained by this procedure can
22 be interpreted as the ratio of observed normalised counts and the counts predicted by the
23 RMLM, and the associated *p*-value provides an interpretable estimate of significance.

24 The DESeq2 analysis pipeline enables the introduction of per-gene, per-sample normalisation
25 factors that are commonly used to correct for batch-dependent GC-content or length biases.
26 We adapted this functionality to normalise the growth rate bias of each gene, by introducing
27 factors N_{ijk} that converted between the measured raw counts c_{ijk} and RMLM-predicted raw
28 counts q_{ijk} :

29
$$q_{ijk} = \frac{c_{ijk}}{N_{ijk}}, \quad (11)$$

1 in analogy to the definition of size factors in Equation (1). However, the fitting of RMLMs
2 yielded per-gene, per-sample predictions p_{ijk} of the normalised counts. Using the sample-
3 dependent size factors, we converted these to predictions of raw counts as follows:

4

$$q_{ijk} = p_{ijk} S_{jk}. \quad (12)$$

5 Therefore, the normalisation factors were calculated as

6

$$N_{ijk} = \frac{c_{ijk}}{S_{jk} p_{ijk}} = \frac{n_{ijk}}{p_{ijk}}. \quad (13)$$

7 We excluded genes with negative predicted raw counts and rescaled the normalisation factors
8 across samples for each gene to have a geometric mean of 1 for numerical accuracy.

9 Using the RMLM-predicted raw counts, we further defined a synthetic reference condition with
10 three biological replicates by using the median predicted count across all growth media for
11 each replicate as follows:

12

$$s_{ik} = \text{int} \left(\text{median}_j q_{ijk} \right). \quad (14)$$

13 These reference counts were rounded to the nearest integer, as they represent raw counts in
14 the DESeq2 pipeline. By design, the q_{ijk} have no residual growth-rate trend.

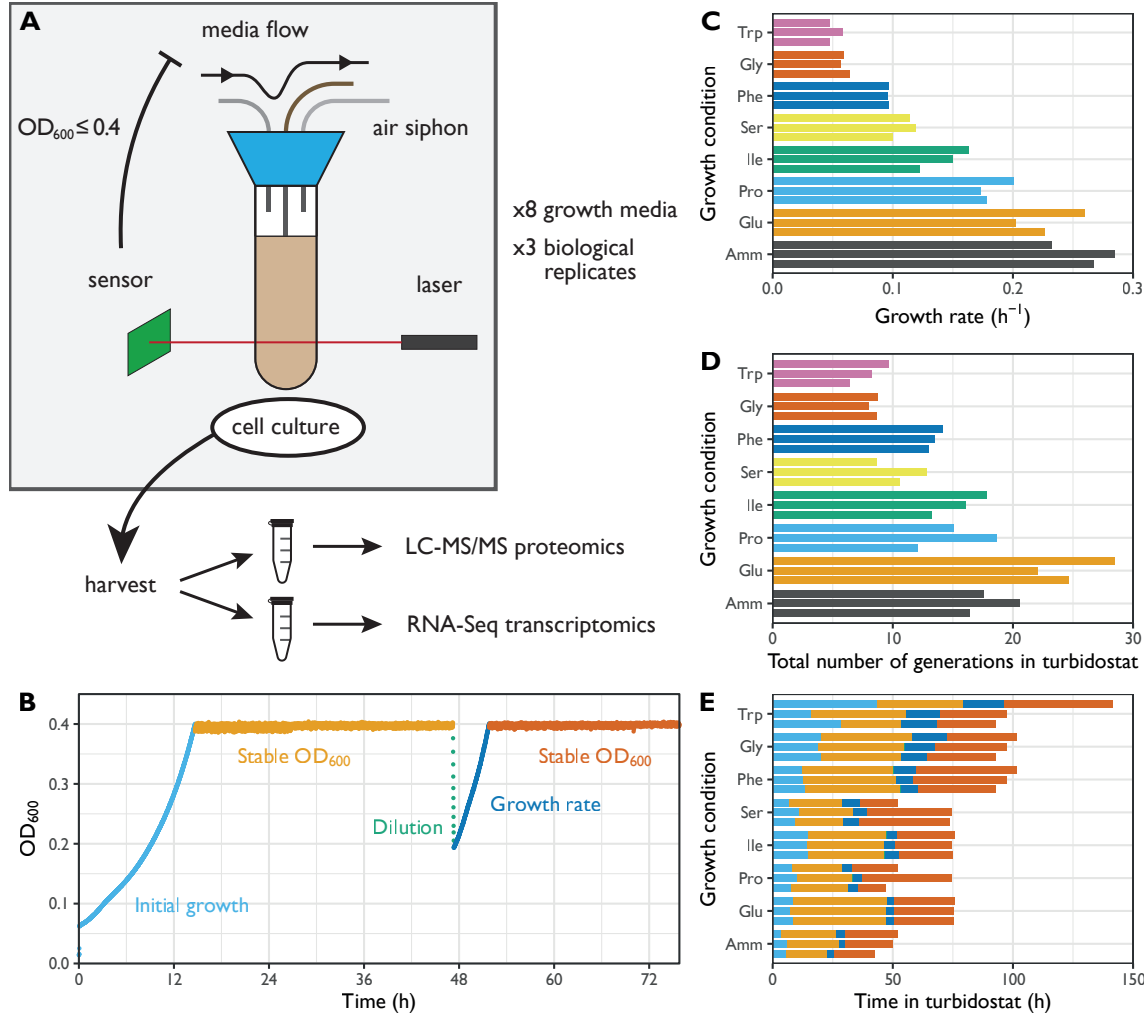
15 Subsequently, the analysis proceeded on the constructed data set with 9 conditions: the
16 original 8 and the synthetic one, with each set having 3 biological replicates. Pairwise fold-
17 changes F and the associated p -values (both uncorrected and adjusted p_{adj}) are reported
18 between the 8 growth media and the synthetic reference. Genes were reported as differentially
19 expressed (DE) if $p_{\text{adj}} < 0.01$ and $|\log_2 F| > 0.5$ for at least one condition.

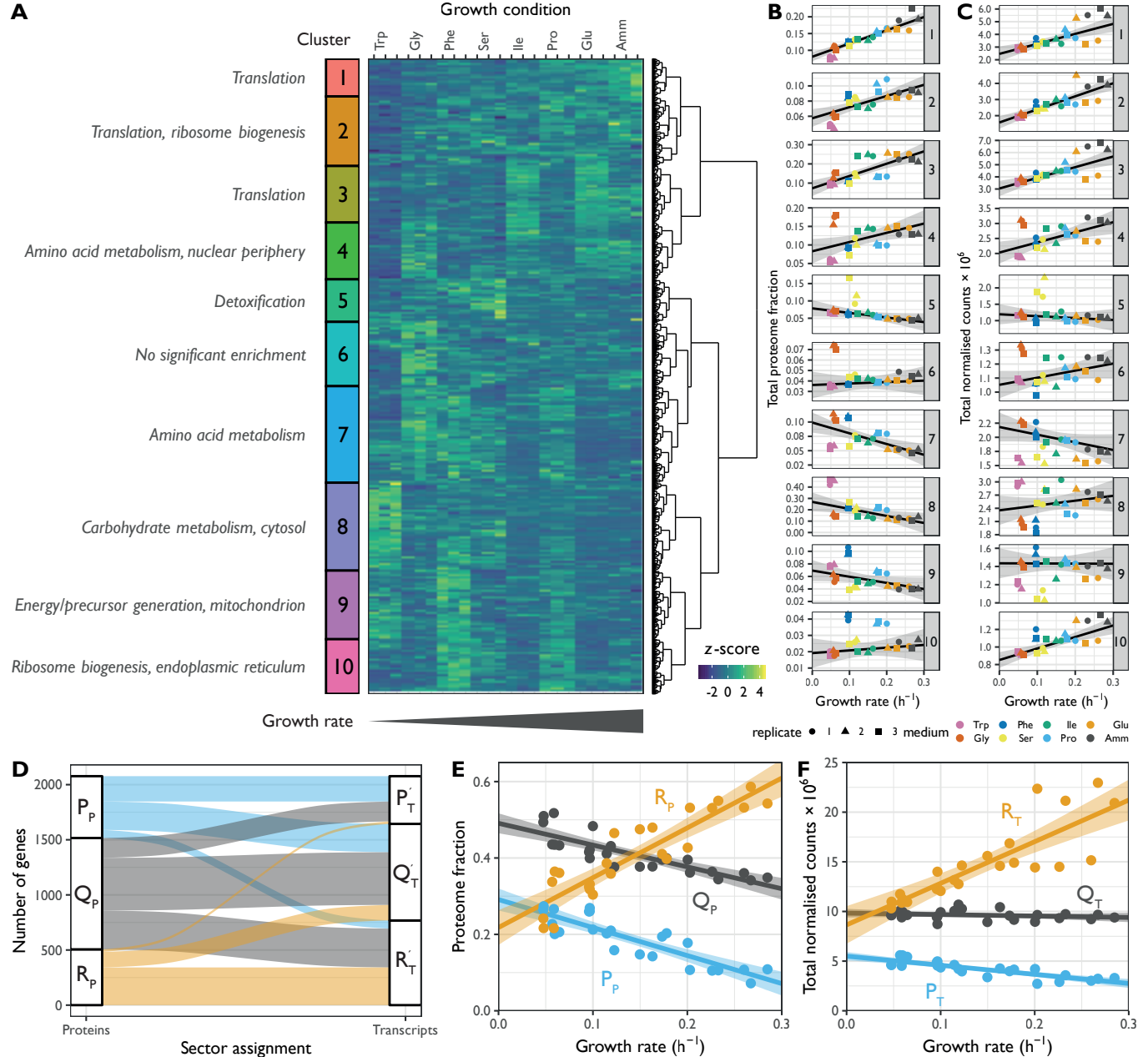
20 **Functional enrichment**

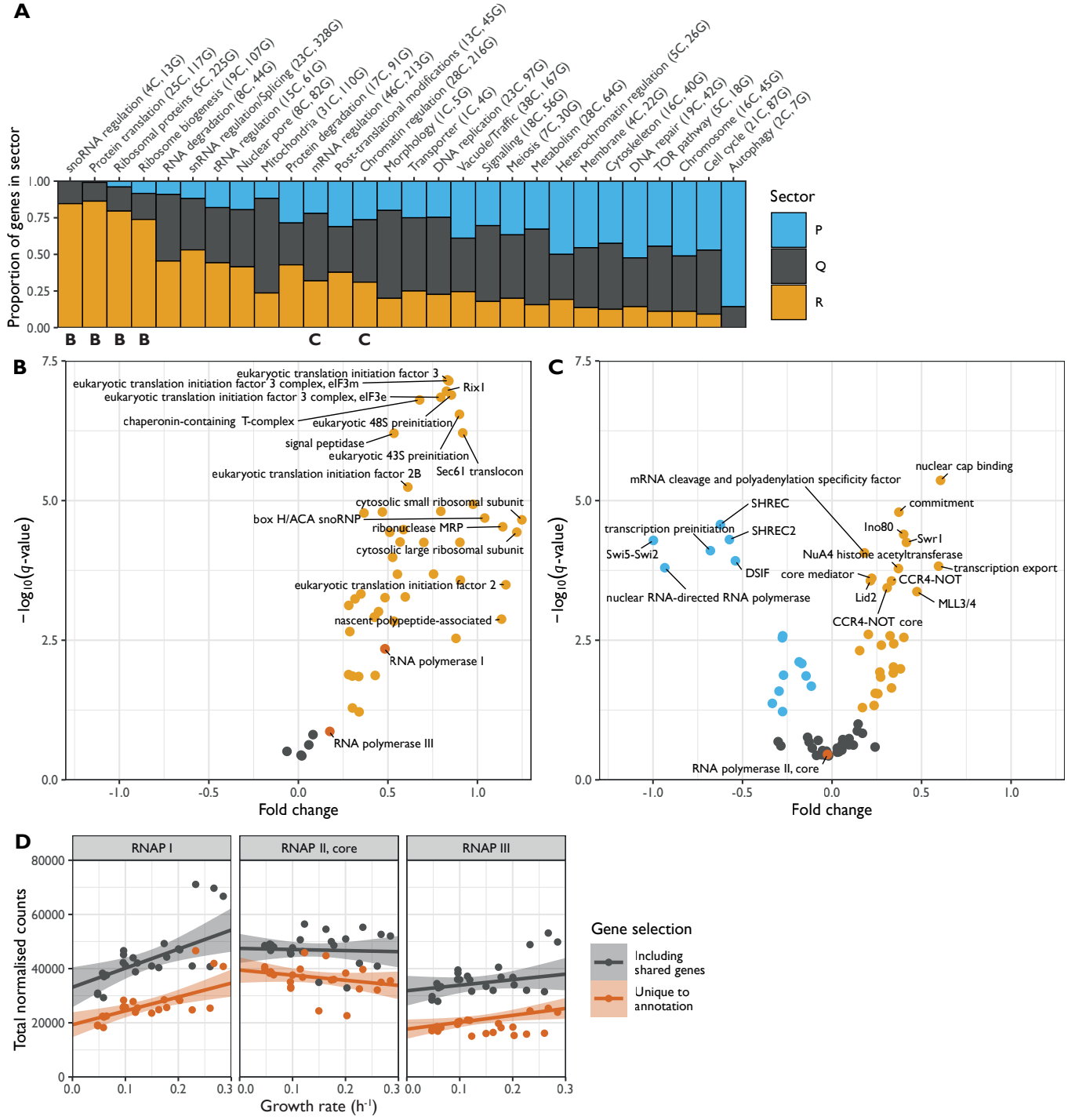
21 We performed one-sided Fisher exact tests to assess the enrichment of DE genes across the
22 *S. pombe* GO-slims and terms from the biological_process GO with at most 50 annotations in
23 *S. pombe* (Gene Ontology Consortium 2019; Lock et al. 2019). From the resulting p -values,
24 local false discovery rates lfd were calculated using the `fdrtool`'s false non-discovery rate
25 method (Strimmer 2008).

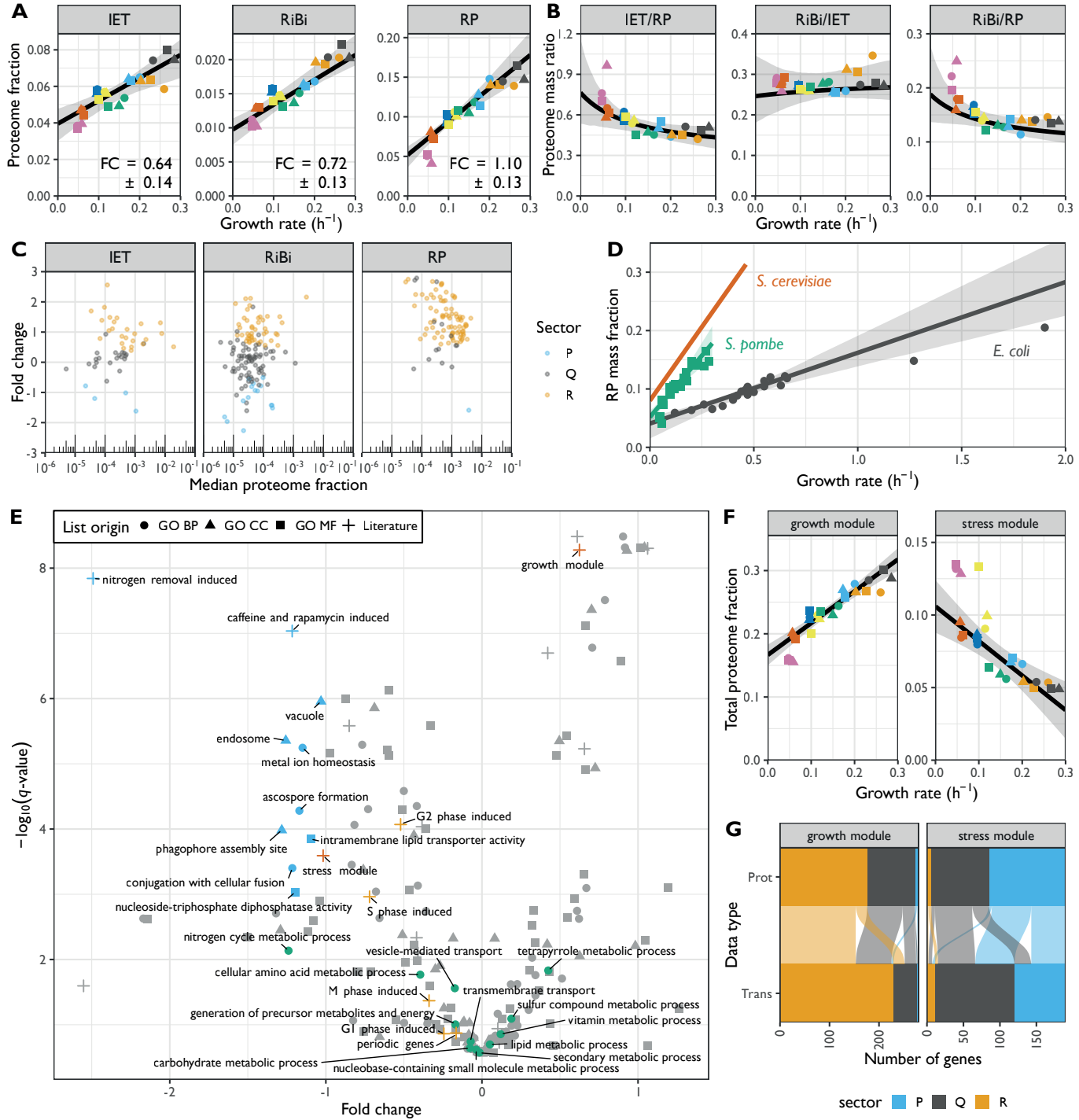
26 In the enrichment plots for the GO-slim terms (**Fig. 6B, Supp. Fig. S2.1**), terms with $lfd < 0.05$
27 were deemed significant, and the terms were ordered from top to bottom by increasing
28 smallest lfd to aid interpretation. For the biological_process enrichment plot (**Supp Fig. S5.3**),
29 the significance threshold was $local fdr < 0.001$. The significant terms were clustered
30 hierarchically using the Euclidean distance and Ward linkage ("ward.D2"), using the `hclust`

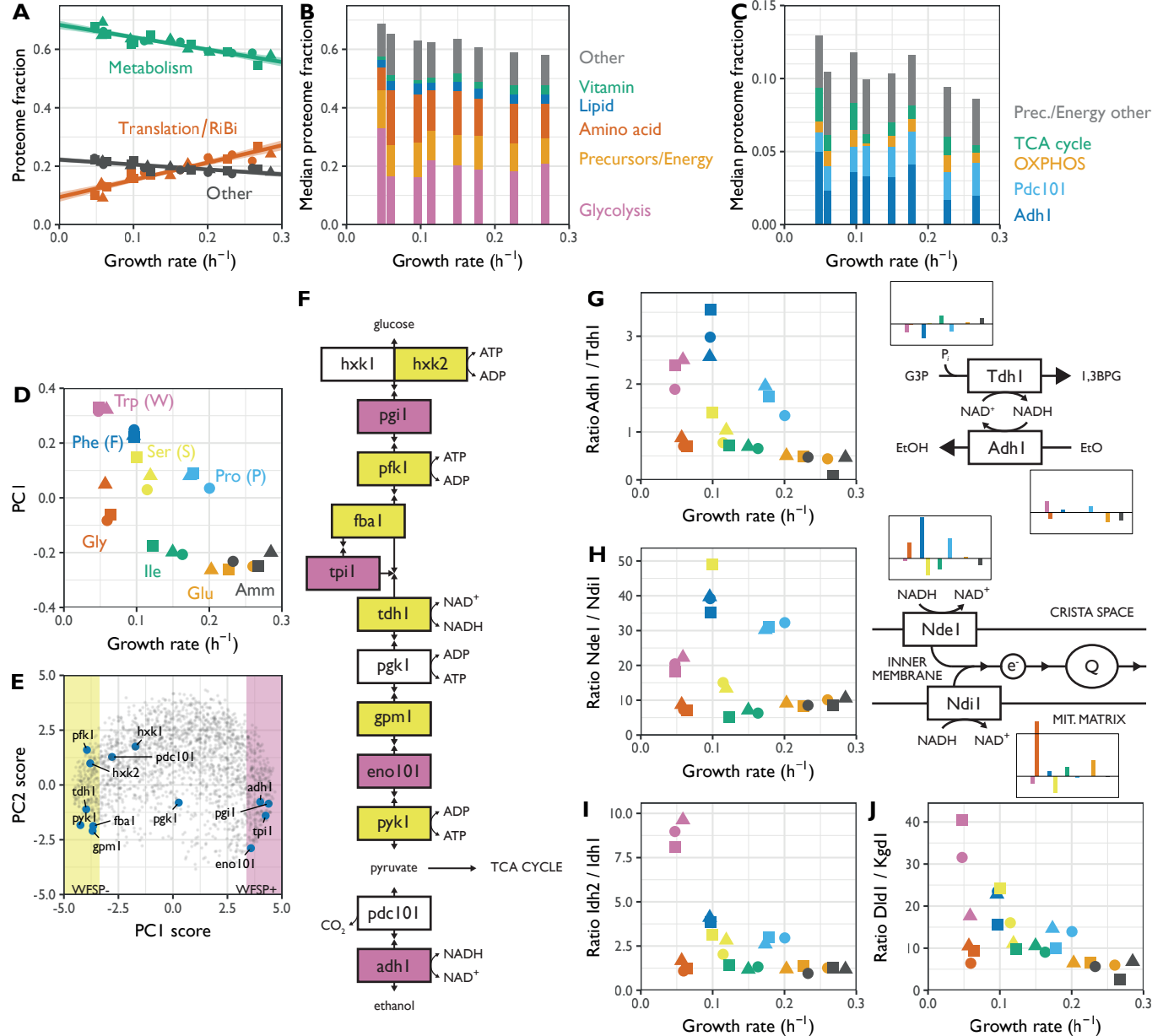
- 1 implementation of the R statistical language (v.3.5.3). The terms were ordered by the smallest
- 2 *lfdr* as much as possible while remaining consistent with the clustering constraint.
- 3

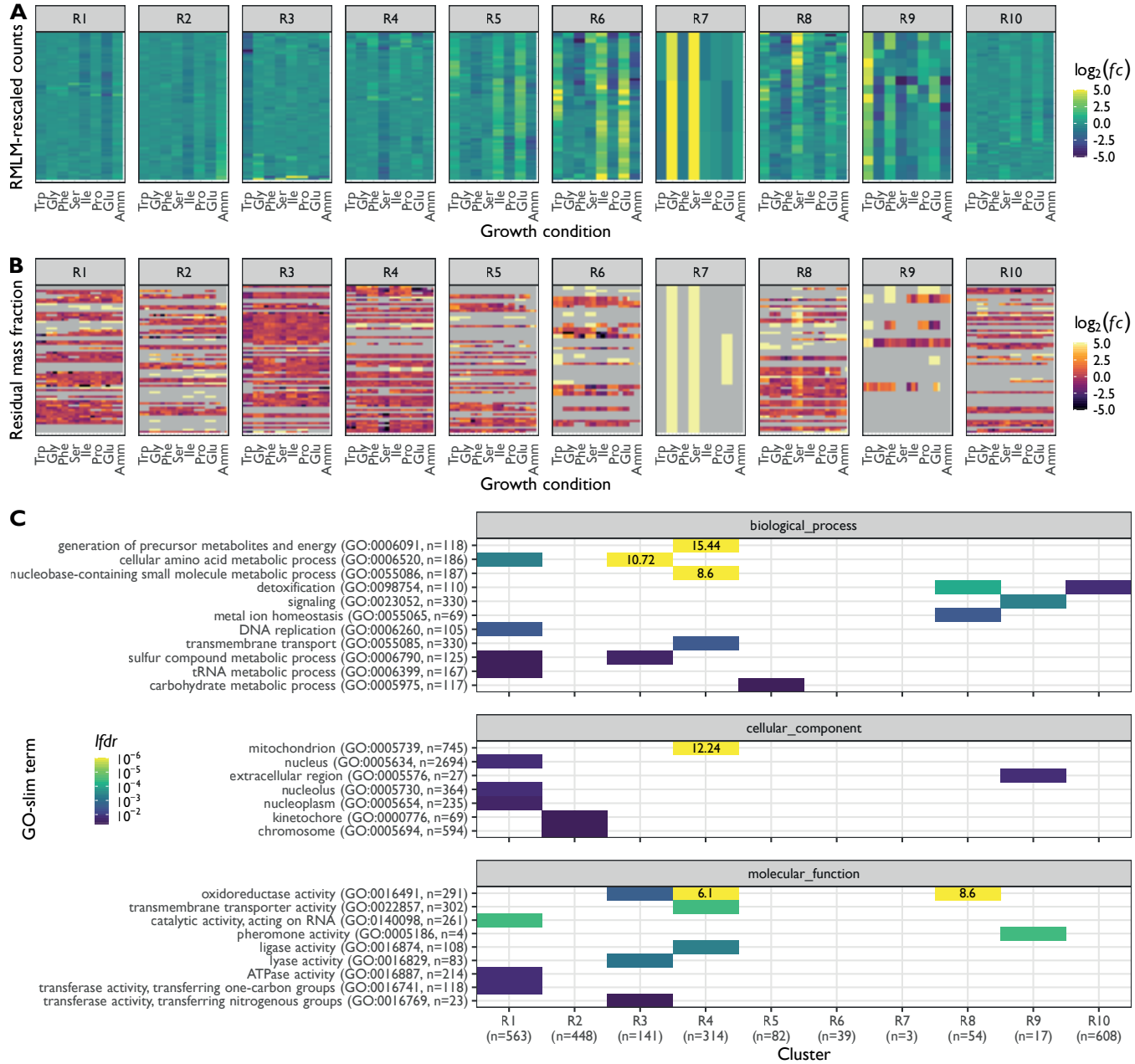


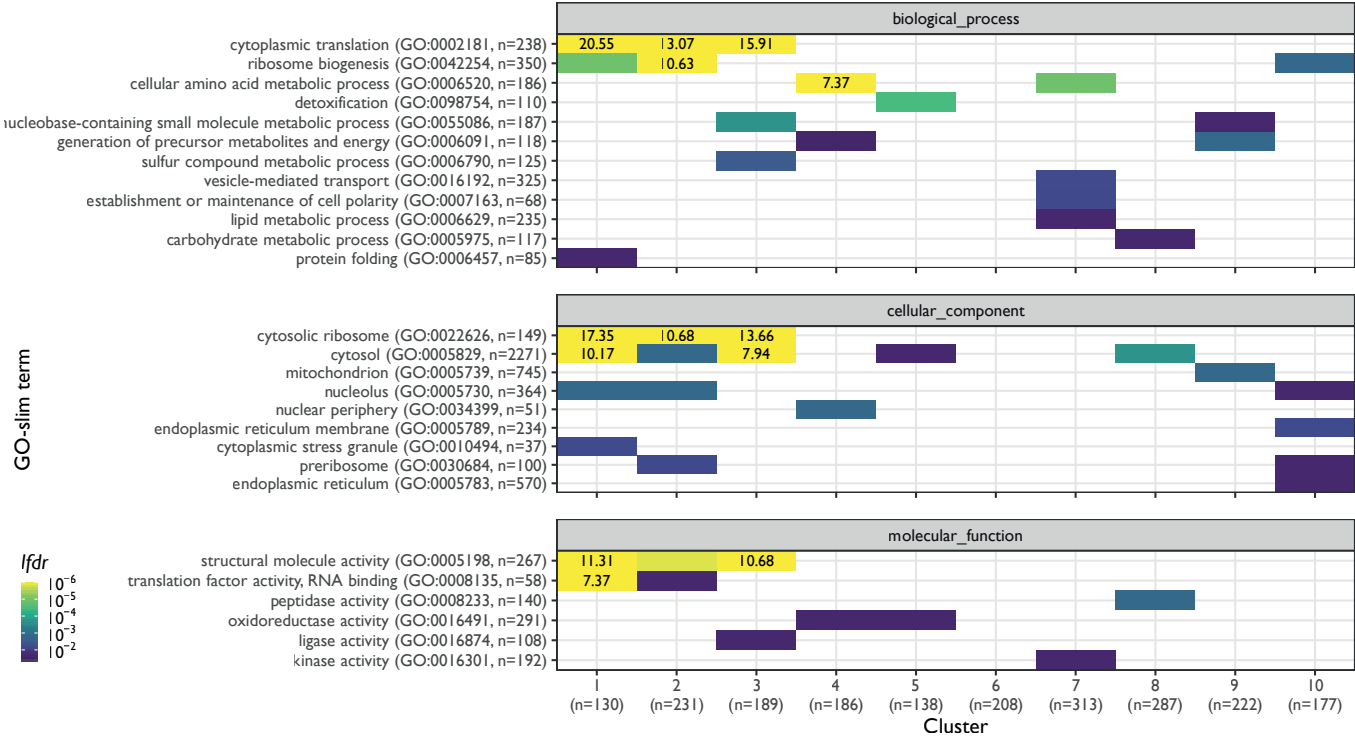


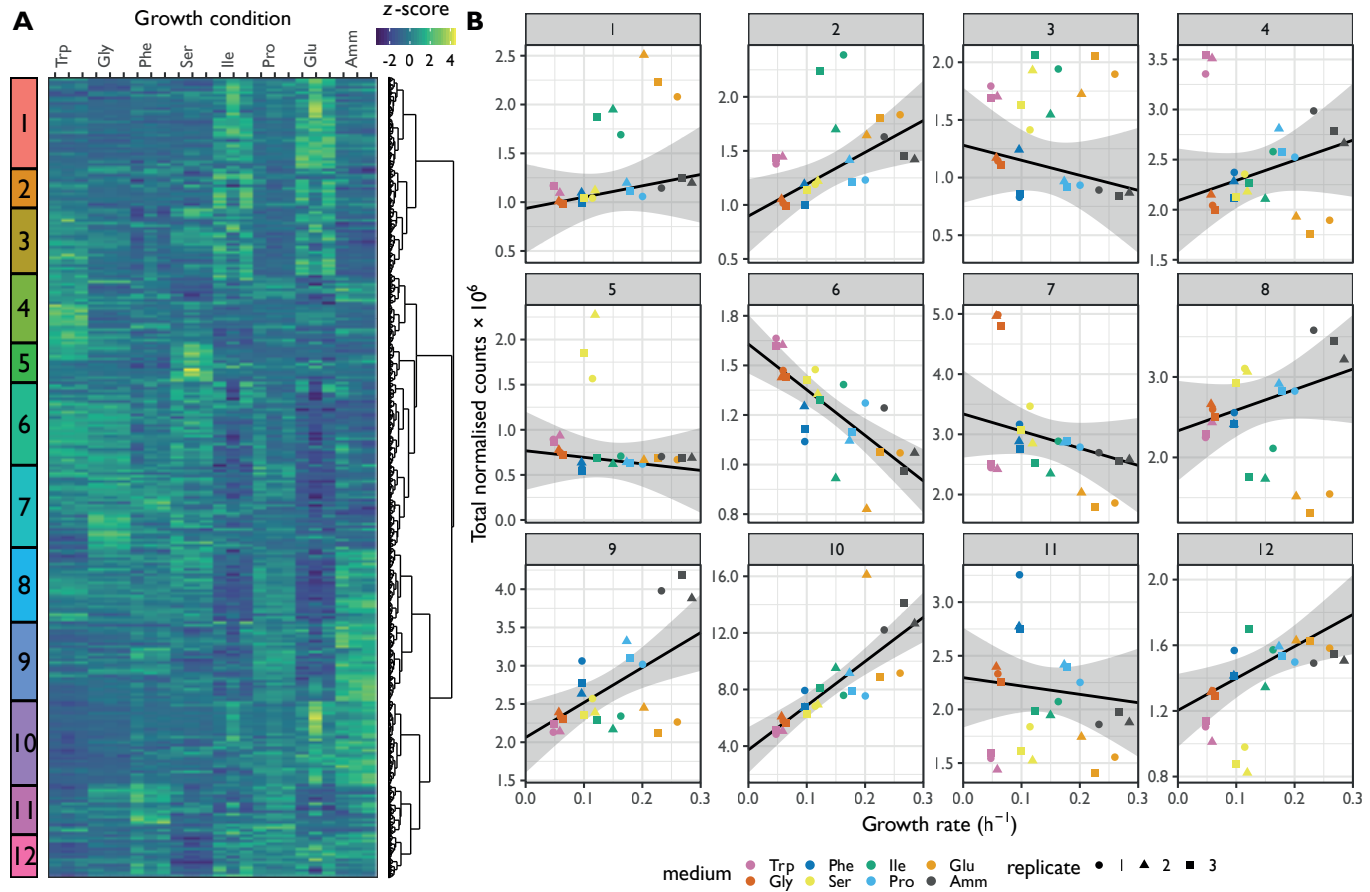


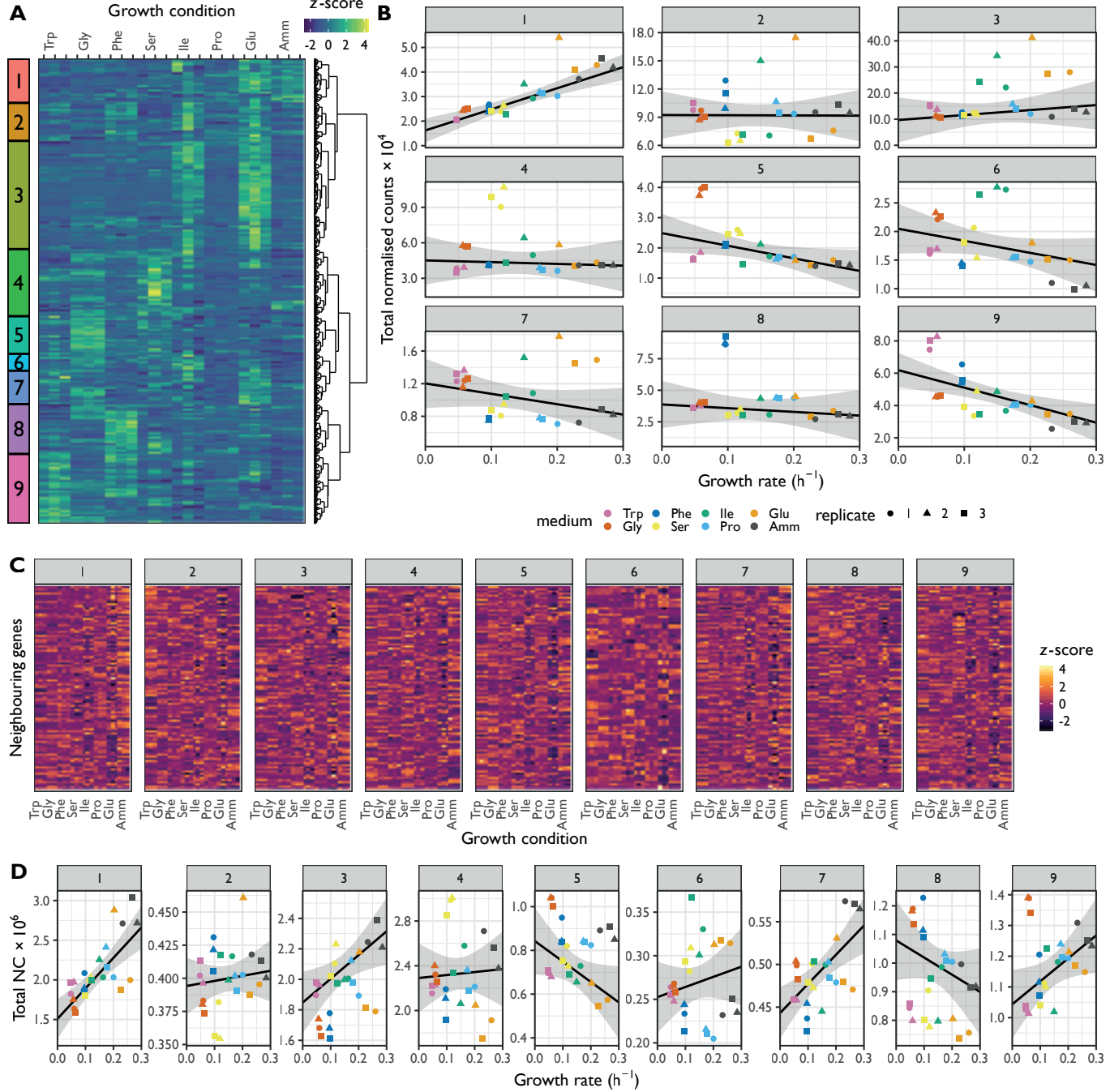


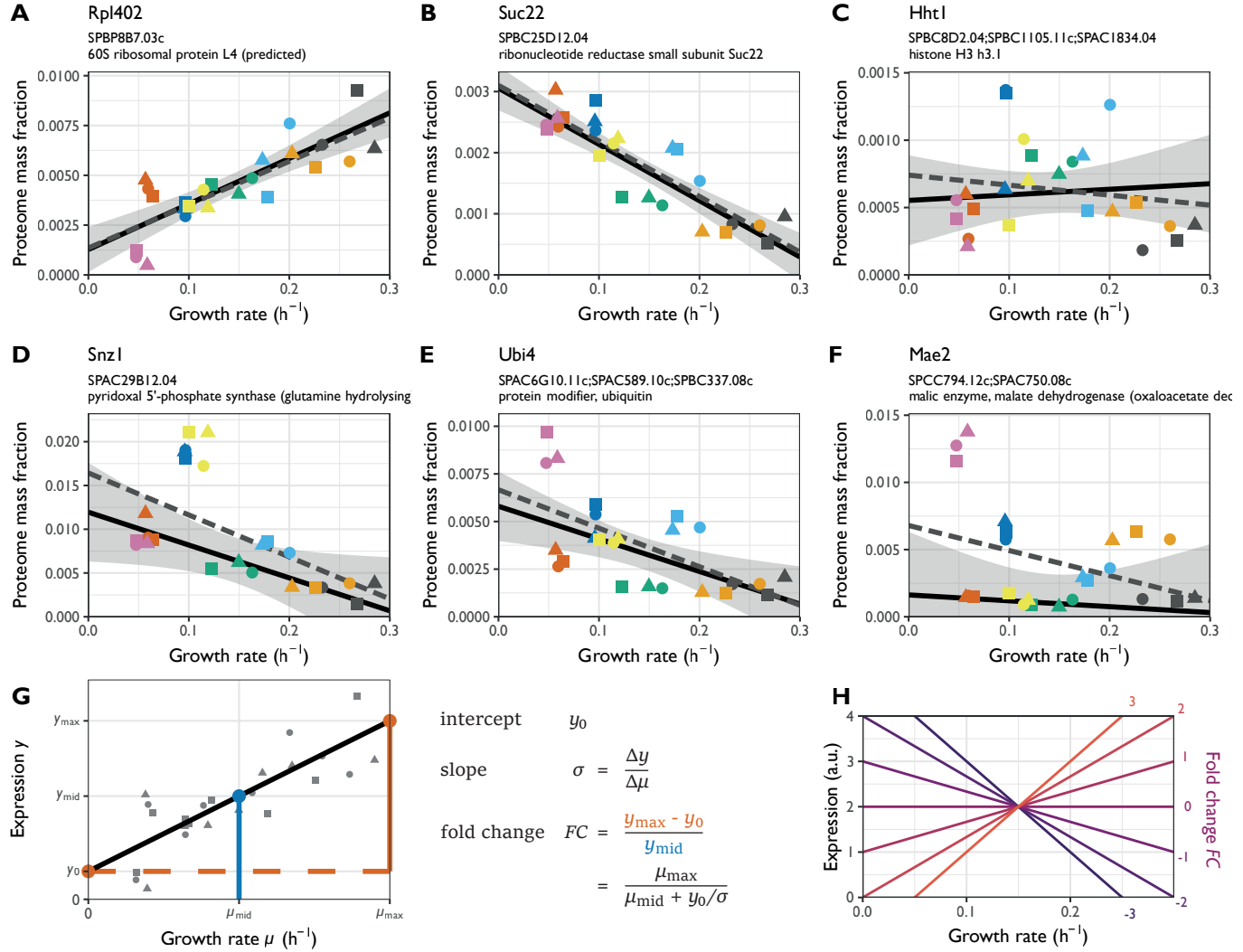












$$\text{fold change } FC = \frac{y_{\max} - y_0}{y_{\min}}$$

$$= \frac{\mu_{\max}}{\mu_{\min} + y_0/\sigma}$$

